The YAP1 isoform, YAP1-2α, promotes oncogenic properties by inducing liquid-liquid phase separation through specific heterodimerization with TAZ

Takuya Ooki[1], Takeru Hayashi[1], Yui Yamamoto[1], and Masanori Hatakeyama[1,2,*]

From the [1]Laboratory of Microbial Carcinogenesis, Institute of Microbial Chemistry, Microbial Chemistry Research Foundation, Tokyo, Japan; [2]Center of Infection-associated Cancer, Institute for Genetic Medicine, Hokkaido University, Sapporo, Japan

***For correspondence: Masanori Hatakeyama, mhata@m.u-tokyo.ac.jp**

Running title

Induction of LLPS by YAP1-2α/TAZ heterodimerization

Keywords

Liquid-liquid phase separation, Cancer biology, Hippo pathway, alternative splicing, epithelial-mesenchymal transition (EMT), Ovarian cancer.

Abstract

The role of alternative splicing in initiating and promoting neoplastic transformation poses a significant challenge to understanding cancer. The pro-oncogenic transcriptional coactivator YAP1 comprises at least eight isoforms, yet the specific and overlapping functions in cancer development remain poorly understood. Here, we show that the YAP1-2 isoform, YAP1-2α, exhibits significantly greater activity in inducing nuclear condensates via liquid-liquid phase separation (LLPS) than other isoforms. Mechanistically, YAP1-2α interacts specifically with its homolog TAZ via the leucine zipper and with TEADs, the primary transcriptional partners of YAP1 and TAZ. The tetrameric complex is further assembled multivalently by BRD4, promoting LLPS. The resulting YAP1-2α/TAZ/TEAD complex binds to super-enhancer elements and strongly enhances pro-oncogenic target gene expression in a BRD4-dependent manner. Cancer cells with higher YAP1-2α levels display a clear EMT signature that drives more malignant traits. Similarly, increased YAP1-2α levels enhance pro-oncogenic features, including sphere formation, extracellular matrix invasion, and resistance to various stresses including anti-cancer drugs. In high-grade serous ovarian cancers (HGSOCs), higher YAP1-2α mRNA levels are associated with nuclear YAP1 biomolecular condensates and more advanced clinical stages. Our study shows that YAP1-2α enhances cancer cell aggressiveness via LLPS, suggesting that the LLPS-induced

1 **YAP1-2α/TAZ/TEAD super-enhancer is a promising target for treating**

2 **refractory cancers.**

3

4

5

6

Introduction

Alternative splicing is a process in which a single gene produces multiple protein products, and its dysregulation is common during the progression of malignant tumors. Abnormal splicing affects key features of cancer, including cell growth, apoptosis, invasion, metastasis, drug resistance, and the immune response (1-3). Therefore, studying protein polymorphisms and their functions arising from alternative splicing during malignant progression may lead to the identification of promising cancer therapeutic targets.

YAP1 and its homolog TAZ lack a DNA-binding domain; instead, they activate downstream transcription by interacting with sequence-specific transcription factors, most notably the TEAD family transcription factors (TEAD1-4) (4, 5). The YAP1/TEAD and TAZ/TEAD complexes integrate signals related to mechanical, metabolic, and cell density to coordinate cell proliferation and differentiation during development and neoplastic progression by activating classical and super-enhancers (6, 7). In cancer cells, elevated levels of YAP1 and TAZ promote cancer stem-like properties by activating epithelial-to-mesenchymal transition (EMT)-inducing transcriptional regulators such as ZEB1 and SNAI2 through TEAD-dependent transactivation (8). Additionally, YAP1 and TAZ contribute to the development of resistance to anticancer drugs (9). In particular, the transcriptional programs mediated by YAP1 and TAZ intersect with the KRAS-ERK MAPK pathway, sharing target genes that confer resistance to RAF and MEK inhibitors across various cancer cells

(10, 11). While YAP1 and TAZ collaborate to control gene expression, their binding sites are not always identical or overlapping (12, 13). One possible reason for these differences may be splicing variants. Unlike TAZ, YAP1 pre-mRNA undergoes complex differential splicing, resulting in at least eight YAP1 isoforms in human cells (14, 15). Indeed, these isoforms exhibit both shared and distinct functions and regulate distinct sets of genes (16). However, the molecular mechanism by which structural variations in these YAP1 isoforms differentially regulate downstream genes remains unknown.

The presence or absence of exon 4, which encodes the second WW domain (WW2), classifies YAP1 into YAP1-1 (with one WW domain) and YAP1-2 (with two WW domains). The WW domain binds proline-rich sequences such as PPxY (17) and is crucial for nuclear translocation (18). There are four additional pre-mRNA splicing variants for both YAP1-1 and YAP1-2 forms. YAP1-1γ and YAP1-2γ mRNAs contain a shorter exon 5 (exon 5.1, missing the β-segment) and exon 6. YAP1-1δ and YAP1-2δ mRNAs feature a longer exon 5 (exon 5.2, including the β-segment) and exon 6 (which encodes the γ-segment). YAP1-1β and YAP1-2β mRNAs contain exon 5.2 but lack exon 6, whereas YAP1-1α and YAP1-2α mRNAs include exon 5.1 but do not have exon 6. YAP1 isoforms can heterodimerize with TAZ via leucine zippers (19). However, the effects of these differences on cancer progression and the mechanisms that underlie them remain largely unexplored. In this work, we show that

heterodimerization of YAP1-2α with TAZ via a leucine zipper triggers liquid-liquid phase separation (LLPS). LLPS is a widespread phenomenon that supports the formation of membrane-less organelles, also known as biomolecular condensates, within cells. These organelles serve as sites for various bioreactions that regulate cellular functions (20, 21). Specifically, LLPS-mediated biomolecular condensation of transcription factors and coactivators within the nucleus is essential for the formation and activation of super-enhancers (22).

Super-enhancers are characterized by high concentrations of transcription factors, coactivators, mediators, and epigenetic modifiers that strongly enhance transcriptional output and integrate multiple signaling pathways that determine cell identity and state (23, 24). Cancer cells adapt to external environments by extensively rewiring their transcriptional networks through super-enhancer formation, which promotes malignant properties by supporting abnormal proliferation signaling, activating anti-apoptotic mechanisms, and facilitating invasion and metastasis. This process enables cancer cells to develop resistance to adverse conditions while creating a tumor-favorable microenvironment, including an immunosuppressive state (25-29). We also demonstrate that YAP1-2α/TAZ-induced LLPS activates TEAD-specific super-enhancers that increase expression of EMT-related genes and promote the development of cancer hallmarks such as sphere formation, invasion, and resistance to various stresses including drug resistance. This study uncovers an unexpected link among YAP1 splicing isoforms, LLPS

1 induction, and the activation of super-enhancers, which contribute to
2 malignant properties. Inhibition of splicing that generates YAP1-2α or
3 disruption of the YAP1-2α/TAZ/TEAD complex may subvert the malignant
4 progression of cancer.
5

Results

YAP1 induces LLPS in a splicing variation-dependent manner

To elucidate the biological differences among eight YAP1 isoforms (Fig. 1*A*; four YAP1-1 isoforms and four YAP1-2 isoforms), we first generated YAP1-knockout (KO) UWB1.289 human high-grade serous ovarian cancer (HGSOC) cells using the CRISPR-Cas9 system. In general, YAP1-1 mRNA expression is substantially lower than that of YAP1-2 across various cell types, especially in cancer cells (30). Consistent with this, YAP1-2 mRNAs were the predominant YAP1 mRNA species in UWB1.289 cells (Fig. 1*B*, lane 1). After single-cell cloning, immunoblot analysis confirmed the absence of endogenous YAP1 proteins (both YAP1-1 and YAP1-2 species) in the cloned YAP1-KO cells (Fig. 1*B*, lane 2). These YAP1-KO cells were expanded and then transiently transfected with expression vectors encoding one of eight YAP1 isoforms, each fused to mVenus at the C-terminus. By western blotting, the overall expression levels of the mVenus-fused YAP1-1 and YAP1-2 isoforms were comparable across the transfected YAP1-KO cells (Fig. 1*B*, lanes 3-10). On the other hand, at the single-cell level, variability in expression levels (range: 500.34 to 15851.8) were observed even within the single isoform (Fig. S1, *A*-*B*). To minimize the influence of this variation in expression, we analyzed YAP1 isoforms in a cell population in which YAP1 expression levels fell within a defined range (mean fluorescence intensity ± SD), as indicated by the gray area in Figure S1B. As a result, cells expressing mVenus-fused YAP1-2α exhibited more nuclear puncta than those

expressing other mVenus-fused YAP1 isoforms (Fig. 1, *C-D*). To exclude the possible influence of the size or location of the protein tag on YAP1-dependent puncta formation, we constructed expression vectors in which an HA tag or an mVenus tag was fused to the N-terminus of YAP1-2 isoforms, the major YAP1 species in the UWB1.289 cell line, and examined their ability to form puncta. The size and location of the tag (HA or mVenus) did not affect puncta formation by the YAP1-2 isoforms (Fig. S1, *C-F*). To test whether puncta formation was due to the overexpression of YAP1, we also established UBW1.289-derived YAP1-KO clone cells reconstituted with HA-tagged YAP1-2α or HA-tagged YAP1-2 α, the levels of which were comparable to those of endogenous YAP1-2 species (Fig. 1*E*). Immunofluorescence staining analysis using an anti-YAP1 antibody revealed that nuclear puncta were easily detectable in YAP1-2α-reconstituted, but not in YAP1-2γ-reconstituted, cells (Fig. 1*F*). This finding indicated that, among eight YAP1 isoforms, YAP1-2α specifically induces puncta formation in the nucleus. The formation of condensates of transcription cofactors within the nucleus is known to alter transcriptional activity by activating super-enhancers via LLPS formation (22-24). Biomolecular condensates formed through LLPS are membrane-less and exhibit liquid-like properties such as droplet fusion and high molecular mobility within the droplet. These properties can be detected via live-cell fluorescence imaging and Fluorescence Recovery After Photobleaching (FRAP) analysis (31). To further elucidate whether YAP1-2α puncta have liquid-like properties or not, we conducted a time-lapse imaging

experiment and FRAP analysis in *YAP1*-KO UWB1.289 cells transfected with mVenus-fused YAP1-2α. Administration of 1,6-hexanediol (Hex), an agent that disrupts liquid-like condensates without affecting solid aggregates, to mVenus-fused YAP1-2α-expressing cells eliminated puncta formation (Fig. 1*G*). In addition to this, YAP1-2α puncta exhibited puncta fusion (Fig. 1*H*), and FRAP analysis revealed that they also form membrane-less puncta (Fig. 1, *I-J*, Fig. S1, *G-J*). Based on these observations, we concluded that YAP1-2α is a YAP1-2 splicing isoform capable of efficiently inducing LLPS in the nucleus.

YAP1-2α/TAZ/TEAD complex is required for LLPS formation

A previous study showed that the leucine zipper in the coiled-coil region of YAP1-2α interacts with the leucine zipper in TAZ's coiled-coil domain, forming a YAP1/TAZ heterodimer (19). Indeed, fluorescence imaging analysis demonstrated that TAZ colocalizes with YAP1-2α puncta (Fig. 2*A*). To determine if the leucine zipper structure of YAP1-2α is crucial for LLPS-induced puncta formation, we created a YAP1-2α leucine zipper mutant (LZM) by substituting the conserved leucine residues with alanine, disrupting its structure. The mutant significantly reduced TEAD reporter activation by YAP1-2α (Fig. S2*A*). In this experiment, the YAP1-2α(S94A) mutant, which fails to activate the TEAD reporter due to impaired binding to TEAD (4), served as a negative control that does not activate the TEAD reporter. A proximity ligation assay (PLA) also confirmed

heterodimerization between YAP1-2α and TAZ in the nucleus as previously reported (19). TAZ also formed a heterodimer with YAP1-2α(S94A) but not with YAP1-2α(LZM), YAP1-2α(LZM|S94A), or YAP1-2γ (Fig. S2*B* upper, S2*C*). As expected, YAP1-2α, YAP1-2α(LZM), and YAP1-2γ interacted with TEAD, while YAP1-2α(S94A) and YAP1-2α(LZM|S94A) did not (Fig. S2*B* lower, S2*D*). Additionally, we examined the ability of these YAP1-2α mutants to undergo LLPS. In this experiment, two different types of cancer cells (UWB1.289 cells and MDA-MB-436 human triple-negative breast cancer (TNBC) cells) were used to avoid the possibility that the observed YAP1-2α LLPS was cell- or tissue-type specific. Expression of mVenus-fused YAP1-2α(LZM) in *YAP1*-KO UWB1.289 cells or MDA-MB-436 cells markedly decreased puncta formation (Fig. 2*B*, Fig. S2, *E-F*). The mVenus-fused YAP1-2α(S94A) also showed markedly less puncta-forming activity than the mVenus-fused YAP1-2α(WT) (Fig. 2*B*, Fig. S2, *E-F*), indicating that both the leucine zipper and the TEAD-binding site of YAP1-2α were required for LLPS formation. Furthermore, YAP1-2α-induced LLPS puncta formation was abolished by knocking out endogenous TAZ in both UWB1.289 and MDA-MB-436 cells (Fig. 2*C*, Fig. S2, *G-J*). Reciprocally, artificially enforced heterodimerization between YAP1-2α(LZM) or YAP1-2γ and TAZ(LZM) induced puncta formation (Fig. 2, *D-E*, Fig. S2, *K-L*), confirming the essential role of YAP1-2α/TAZ heterodimerization in YAP1-2α-induced LLPS/puncta formation.

To determine whether the TEAD transcription factors (TEAD1-4), the prevalent partners of YAP1-2α and TAZ in transcriptional regulation, are required for LLPS-mediated nuclear puncta formation, we expressed mVenus-fused YAP1-2α (wild-type, LZM, S94A) in parental UWB1.289 cells. Immunofluorescence staining showed that wild-type YAP1-2α, but not the LZM or S94A mutant, colocalized with TEADs in nuclear puncta (Fig. 2*F*). Moreover, K-975, a selective inhibitor of the interaction between TEAD and YAP1 or TAZ (32), abolished puncta induction by YAP1-2α (Fig. 2*G*, Fig. S2*M*). Thus, YAP1-2α-induced nuclear condensates contained YAP1-2α, TAZ, and TEAD complexes. In this regard, YAP1-2α(S94A) also formed puncta independently of TEAD binding, though less efficiently (Fig. 2, *F*-*G*), suggesting potential TEAD-independent mechanisms for weak condensate formation by YAP1-2α.

TAZ also forms a homodimer via the leucine zipper, leading to LLPS independently of YAP1 and TEAD (33). In contrast, YAP1 cannot form homodimers (19). TAZ/TAZ-LLPS condensates were similarly produced in both parental and *YAP1*-KO UWB1.289 cells (Fig. S2*N*). PLA was used to visualize the interaction between TEAD and HA-tagged YAP1-2α or TAZ. This technique allowed us to distinguish between YAP1-2α/TAZ-LLPS condensates and TAZ/TAZ-LLPS condensates (Fig. S2*O*). Most YAP1-2α-TEAD complexes were localized within YAP1-2α/TAZ-induced LLPS condensates (Fig. S2*O*, right), whereas TAZ-TEAD complexes were located mostly outside TAZ/TAZ-induced LLPS condensates (Fig. S2*O*,

left). This indicates the essential requirement of TEAD in YAP1-2α/TAZ -LLPS, while TAZ/TAZ-induced puncta likely contain other transcription factors. Indeed, TAZ/TAZ homodimers were present in TAZ/TAZ-LLPS but absent in YAP1-2α/TAZ-LLPS (Fig. 2*H*). These findings demonstrate that YAP1-2α/TAZ-LLPS is distinct from TAZ/TAZ-LLPS, the former being formed by YAP1-2α, TAZ, and TEAD complex (YAP1-2α/TAZ/TEAD-LLPS), and the latter by TAZ homodimer without YAP1 and TEAD (TAZ/TAZ-LLPS).

Mechanism of LLPS induction by YAP1-2α/TAZ/TEAD complex formation

Although the ability was much weaker than that of YAP1-2α, YAP1-1α was also capable of forming nuclear puncta (Fig. 1, *C-D*). Since YAP1-1α retains the ability to form a heterodimer with TAZ via the leucine zipper (Fig. S3*A*), factors other than heterodimerization with TAZ may also influence the magnitude of LLPS induction by YAP1-2α. Since YAP1-2α possesses two WW domains, whereas YAP1-1α possesses one WW domain (Fig. 1*A*), we assumed that molecules that interact with the WW domain may determine the difference in LLPS induction between YAP1-1α and YAP1-2α. The WW domain is a protein motif that preferentially binds proline-containing sequences, such as the PPxY and LPxY motifs (17, 34). LLPS enables the formation of membrane-less puncta or droplets in which specific proteins are concentrated via multivalent interactions

(35). Nuclear puncta/condensates formed via LLPS, including transcription factors, coactivators, and mediators like BRD4 and MED1, are associated with the formation of super-enhancers. Thus, greater accumulation of BRD4 in nuclear LLPS condensates is crucial for the formation of stronger super-enhancers (36). Mediators serve various roles in transcription, including linking transcription factors to RNA polymerase II (Pol II) (37). Indeed, in *YAP1*-KO UWB1.289 cells reconstituted with HA-YAP1-2α, as shown in Figure 1*E*-*F*, YAP1-2α puncta co-localized with Pol II (Fig. S3*B*). FRAP analysis of YAP1-2α puncta in *YAP1-KO* UWB1.289 or MDA-MB-436 cells revealed a diffusion coefficient "*D*" of 0.01-0.02 $\mu m^2/s$ (Fig. 1*J*, Fig. S1*I*). It has been reported that the apparent diffusion coefficient within BRD4/MED1 condensates (0.01-0.1 $\mu m^2/s$) is significantly lower than that of free diffusion (0.1-1 $\mu m^2/s$). These findings support the idea that YAP1-2α/TAZ-induced LLPS is associated with super-enhancer formation (22, 38). The function of BRD4 in LLPS relies on two bromodomains binding to H3K27ac, a marker of active enhancers (39). Since BRD4 contains an LPxY motif (LPDY) in bromodomain I and a PPxY motif (PPTY) in its C-terminal proline-rich region (Fig. 3*A*), we hypothesized that these motifs interact with the two WW domains of YAP1-2α, thereby facilitating multivalent protein-protein interactions. Co-immunoprecipitation and PLA studies confirmed a direct interaction between YAP1-2α and BRD4 in both UWB1.289 and MDA-MB-436 cells. This interaction was impaired when either the PPxY or

LPxY motif in BRD4 was disrupted and abolished when both motifs were disrupted (Fig. 3, *B*-*C*, Fig. S3*C*). The significance of BRD4 in YAP1-2α/TAZ/TEAD-LLPS condensates was verified by the results showing that shRNA-mediated BRD4 knockdown in UWB1.289 or MDA-MB-436 cells (Fig. 3, *D*-*E*) and competitive inhibition of the YAP1-BRD4 interaction by an mCherry-fused PPTY peptide derived from the BRD4 sequence in UWB1.289 cells (Fig. S3, *D*-*E*) abolished puncta formation. The reduction in YAP1-2α/TAZ/TEAD-LLPS puncta due to BRD4 knockdown was rescued by ectopic expression of shRNA-resistant wild-type BRD4, but not by BRD4 lacking one or both PPxY/LPxY motifs (Fig. 3*F*, Fig. S3, *F*-*G*). To assess the necessity of the two WW domains in YAP1-2α for effective puncta formation, we disrupted one or both WW domains by introducing point mutations. However, as reported previously (18), these mutants failed to enter the nucleus and accumulated in the cytoplasm (Fig. S3, *H*-*I*). To address this, we used the YAP1 (S127A) mutant, which enters the nucleus due to the Ser127-to-Ala substitution, thereby preventing LATS1/2-mediated phosphorylation that enforces cytoplasmic retention of YAP1 (4). We then introduced these point mutations into the WW domains of YAP1-2α(S127A). Experiments with these YAP1 mutations revealed that loss of function in one of the two WW domains in YAP1-2α significantly reduced its binding to BRD4 (Fig. 3*G*, Fig. S3*J*) and drastically diminished puncta formation (Fig. 3*H*, Fig. S3*J*) in UWB1.289 cells. Consistent with this, the BRD4-binding affinity of YAP1-1α, which

possesses only a single WW domain and exhibits substantially weaker LLPS-forming ability than YAP1-2α, was significantly lower than that of YAP1-2α (Fig. S3, *K-M*). These findings indicate that the interactions between BRD4's PPxY/LPxY motif and YAP1's WW domains are crucial for generating YAP1-2α/TAZ/TEAD-induced LLPS condensates.

YAP1-2α/TAZ/TEAD complex binds to TEAD-positive super-enhancer elements and reinforces gene expression

To investigate whether LLPS formation via heterodimerization of YAP1-2α and TAZ effects gene expression, we first confirmed typical TEAD target gene, *CCN1* (*Cyr61*) and *CCN2* (*CTGF*), expression levels in YAP1-2 isoforms transfected UWB1.289 cells. YAP1-2 isoforms increased *CCN2* mRNA expression to a similar degree (Fig. S4, *A-B*), whereas YAP1-2α significantly elevated *CCN1* mRNA expression compared to other isoforms (Fig. 4*A*). The increase in *CCN1* mRNA, but not *CCN2* mRNA, was abolished by *TAZ* knockout (Fig. 4*B*, Fig. S4, *C-D*). Notably, even in *TAZ*-KO cells, elevated YAP1-2α increased *CCN1* mRNA expression, albeit to a lesser extent (Fig. 4*B*). Similarly, YAP1-2α(LZM), which cannot form a heterodimer with TAZ, still retained the ability to induce *CCN1* mRNA, though much less efficiently than YAP1-2α(WT) (Fig. 4*C*, Fig. S4*E*). Hence, like other YAP1 isoforms, the YAP1-2α/TEAD complex can transactivate the *CCN1* gene in an LLPS-independent manner without TAZ. Conversely, artificial YAP1-2α/TAZ heterodimerization, as shown in

Figure 2E, enhanced *CCN1* gene expression (Fig. 4*D*), indicating that YAP1-2α/TAZ heterodimerization, which induces LLPS, is crucial for robust induction of TEAD-dependent gene expression.

Since LLPS-mediated nuclear condensate formation is closely associated with transcriptional regulation via super-enhancer induction (22), we hypothesized that the YAP1-2α/TAZ/TEAD complex stimulates potential super-enhancer elements. To test this possibility, we analyzed the identified super-enhancer elements upstream of the *CCN1* and *CCN2* genes using public super-enhancer database SEdb3.0 (http://www.licpathway.net/sedb). Super-enhancer elements in serous ovarian cancer cells (40) and triple-negative breast cancer cells (41) were identified from active enhancer maker H3K27ac ChIP-seq datasets using ROSE (Rank Ordering of Super-Enhancers) algorithm. Consistent with aforementioned results, identified super-enhancer elements were present upstream of the *CCN1* gene but not *CCN2* (Fig. 4*E*, Fig. S4*F*). Additionally, these elements contain TEAD-binding sites, which led us to focus on these regions as potential super-enhancers that could be activated by the YAP1-2α/TAZ/TEAD-LLPS. Using YAP1-2-reconstituted cells described in Figure 1*E*-*F*, we tested the enrichment of BRD4, a super-enhancer marker (22, 36), along with YAP1, TAZ, and TEAD at the predicted TEAD-positive enhancer region upstream of *CCN1*. In cells ectopically expressing YAP1-2α, the levels of BRD4, YAP1, TAZ, and TEAD were significantly enriched in the upstream regions of *CCN1* [-0.3 kb from the transcription start site (TSS), -0.85 kb from TSS] compared to cells

ectopically expressing YAP1-2γ (Fig. 4*F*). Furthermore, ChIP-re-chip analysis corroborated that the YAP1-2α/TAZ complex was bound to these regions in a TEAD-dependent manner (Fig. 4, *G*-*H*), indicating that the YAP1-2α/TAZ/TEAD complex was specifically bound to the super-enhancer elements along with BRD4. Consistently, increased *CCN1* expression by YAP1-2α was suppressed using JQ1 (Fig. 4*I*, Fig. S4*G*), a selective inhibitor of BRD4-regulated super-enhancers (42). These results provided strong evidence that the YAP1-2α/TAZ/TEAD complex specifically activated the super-enhancer.

YAP1 splicing switch is associated with the EMT signature in HGSOC

To investigate differences in gene expression profiles in same cancer species expressing differential levels of *YAP1* splice variants, we analyzed RNA-seq data from high-grade serous ovarian cancer (HGSOC) in the TCGA public database (43-45). Information on *YAP1* mRNA splicing variant PSI (percent spliced in index) data was obtained from TCGA SpliceSeq (46). Expression of *YAP1* isoforms were defined as "*YAP1-*$\alpha^{dominant}$" [PSI (*YAP1-exon 6*) < median, PSI (*YAP1-exon 5.2*) < median], "*YAP1-*$\beta^{dominant}$" [PSI (*YAP1-exon 6*) < median, PSI (*YAP1-exon 5.2*) > median], "*YAP1-*$\gamma^{dominant}$" [PSI (*YAP1-exon 6*) > median, PSI (*YAP1-exon 5.2*) < median], or "*YAP1-*$\delta^{dominant}$" [PSI (*YAP1-exon 6*) > median, PSI (*YAP1-exon 5.2*) > median]. With this HGSOC subgrouping, 754 genes were significantly upregulated in the *YAP1-*$\alpha^{dominant}$ group compared to the

1 *YAP1-$\gamma^{dominant}$* group (Fig. 5*A*). On the other hand, 146 genes were
2 upregulated in the *YAP1-$\gamma^{dominant}$* group, indicating that *YAP1-$\alpha^{dominant}$*
3 group is transcriptionally more active than the *YAP1-$\gamma^{dominant}$* group. The
4 finding is totally consistent with the fact that super-enhancer activation is
5 characterized by the activation of a greater number of genes. Hallmark
6 gene set analysis revealed that the elevated 754 genes were substantially
7 associated with EMT and angiogenesis (Fig. 5*B*). In particular, EMT-
8 associated genes (*SNAI2*, *SPARC*) (8, 47) and *ALDH1A3*, a marker of cancer
9 stem-like cells (48), were significantly elevated in the *YAP1-$\alpha^{dominant}$*
10 group compared to other groups without an increase in *YAP1* and *TAZ*
11 mRNA levels (Fig. S5*A*). In this regard, previous reports have shown that
12 YAP1 regulates the gene expression of *SNAI2* (8), *ALDH1A* (49), and
13 *SPARC* (50). Furthermore, these genes have been shown to enhance EMT,
14 acquisition of cancer stem cell-like properties, drug resistance, and
15 invasion in cancer cells, including serous ovarian cancer (51-53). Indeed,
16 YAP1-2α-expressing UWB1.289 cells exhibited significantly increased
17 gene expression of *SPARC*, *ALDH1A3*, and *SNAI2* compared to YAP1-2γ-
18 expressing cells (Fig. 5*C*, Fig. S5*B*). Notably, treatment with the BRD4
19 inhibitor JQ1 inhibited LLPS-mediated YAP1-2α puncta formation and
20 suppressed the increased expression of *SPARC* and *ALDH1A3* by YAP1-2α
21 (Fig. 5, *C-D*), suggesting that YAP1-2α potentially activates these genes
22 by stimulating the YAP1-2α/TAZ/TEAD super-enhancers. Therefore, we
23 further investigated the TEAD-positive super-enhancer elements upstream

of the *ALDH1A3* and *SPARC*, revealing the presence of potential super-enhancer elements (Fig. S5*C*). To verify whether YAP1/TAZ/TEAD/BRD4 enriches at the potential super-enhancer elements in an YAP1 isoform dependent-manner, especially between YAP1-2α (which forms efficient LLPS) and YAP1-2γ (which does not form efficient LLPS), we used YAP1-reconstituted cells to evaluate the enrichment of BRD4, YAP1, TAZ, and TEAD in potential TEAD-positive super-enhancer elements upstream of the *SPARC* and *ALDH1A3*. Cells expressing only YAP1-2α exhibited significant enrichment of super-enhancer marker (BRD4), TAZ, and TEAD, along with YAP1, in the predicted TEAD-positive super-enhancer elements upstream of the *SPARC* (-0.67 kb, -3.2 kb from TSS) and *ALDH1A3* (-0.52 kb from TSS). In contrast, this enrichment was not observed in cells ectopically expressing YAP1-2γ (Fig. 5*E*, Fig. S5*D*). The elevated expression levels of *SPARC* and *ALDH1A3* in UWB1.289 cells with ectopic overexpression of YAP1-2α were suppressed by *TAZ* knockout (Fig. 5*F*). Of note, when only TAZ was overexpressed, the expression of these genes decreased rather than increased, even under conditions that enhance the expression of typical TEAD target genes. (Fig. S5, *E*-*F*). These findings suggested that, during LLPS formation initiated by YAP1-2α and TAZ heterodimerization, the splicing switch from YAP1-2γ to YAP1-2α serves as a rate-limiting step, robustly potentiating YAP1-2α/TAZ/TEAD super-enhancers to activate genes associated with EMT and cancer stem-like properties.

1

2 ***YAP1-2α-induced LLPS enhances cancer hallmarks and correlates with***

3 ***malignant grades of HGSOC***

4 The aforementioned results indicated that the splicing switch from YAP1-

5 2γ to YAP1-2α activates EMT through transcriptional reprogramming.

6 EMT potentiates cancer stem-like properties and is characterized by

7 elevated robustness and stiffness of cancer phenotypes, exemplified by

8 "Hallmarks of cancer", contributing to increased invasion, metastasis,

9 resistance to oxidative stress, including ferroptosis and resistance to

10 various cancer therapies (54, 55). Since malignant progression of cancer

11 cells is correlated with enhanced 3D spheroid culture (56), we compared

12 the sphere-forming capacity of YAP1-2α-overexpressing UWB1.289 cells

13 with that of YAP1-2γ-overexpressing UWB1.289 cells. In 2D culture, both

14 YAP1-2α- and YAP1-2γ-overexpressing cells slightly enhanced cell

15 proliferation compared to control cells. However, there was no substantial

16 difference in proliferation between cells overexpressing YAP1-2α and

17 YAP1-2γ. (Fig. S6*A*, left panel). In striking contrast, in 3D culture, the

18 anchorage-independent growth of YAP1-2α-overexpressing cells was

19 much greater than that of YAP1-2γ-expressing cells (Fig. S6*A*, right panel).

20 The enhanced sphere-forming capacity of cells overexpressing YAP1-2α

21 was suppressed by treatment with K-975 or JQ1 (Fig. 6*A*). YAP1-2α-

22 overexpressing cells also showed more aggressive characters, including

23 elevated chemotaxis (Fig. 6*B*, Fig. S6*B,* left), increased invasion into the

extracellular matrix (Fig. 6*C*, Fig. S6*B,* right), and enhanced resistance to oxidative stress such as ferroptosis (Fig. 6*D*) in a TEAD/BRD4 dependent manner. Resistance of cancer cells to ferroptosis is associated with cellular resistance to anti-cancer drugs, including VEGF inhibitors, EGFR inhibitors, and genotoxic reagents (57). Consistently, YAP1-2α-overexpressing cells exhibited elevated resistance to various anticancer agents, including molecular targeted drugs (Trametinib) and genotoxic drugs (Cisplatin, Olaparib) (Fig. 6*E*, Fig. S6*C*). Notably, the aforementioned phenotypes were suppressed by BRD4 inhibition and TEAD inhibition, suggesting that at least the activation of super-enhancers by YAP1-2α contributes to the acquisition of malignant properties in UWB1.289 cells.

To further investigate the impact of YAP1-2α-induced LLPS on oncogenic properties, we again used the artificial heterodimerization system as shown in Figure 2*D*-*E*. To this end, we examined the requirement for YAP1-2α/TAZ heterodimerization to potentiate the oncogenic properties of UWB1.289 cells and the effects of YAP1-2α puncta formation caused by the interaction between YAP1-2α/TAZ and BRD4. Artificial heterodimerization between YAP1-2α(S127A-LZM)-WW1/2^{WT} or YAP1-2α(S127A-LZM)-WW1/2^{mut} and TAZ(LZM) clearly demonstrated the formation of nuclear puncta that is induced by YAP1-2α/TAZ heterodimerization and YAP1-2α/BRD4 interactions (Fig. 6*F*, Fig. S6, *D*-*E*). Under these conditions, malignant properties of cells, such as

1 anchorage-independent growth (Fig. 6*G*), chemotaxis (Fig. 6*H*), matrix
2 invasion (Fig. 6*I*), and resistance to various stresses (Fig. 6, *J*-*K*, Fig. S6*F*),
3 were substantially potentiated by the formation of YAP1-2α/TAZ-induced
4 puncta, indicating the critical role of YAP1-2α/TAZ LLPS-induced puncta
5 formation in increasing the malignant grade of tumor cells.

6 Using clinical cancer specimens, we also investigated the association
7 between *YAP1-2α* expression, nuclear puncta formation, and malignant
8 progression of tumor cells. To assess *YAP1-2α* expression levels in human
9 cancer specimens, a BaseScope probe specific for *YAP1-2α* mRNA was
10 designed. Probe specificity was confirmed using *YAP1*-KO UWB1.289
11 cells that ectopically expressed YAP1-2 isoforms (Fig. S6*G*). BaseScope
12 and immunohistochemistry analyses showed a significant correlation
13 between higher *YAP1-2α* expression and a greater number of YAP1 nuclear
14 condensates in HGSOC patients (Fig. 6, *L*-*N*, Fig. S6, *H*-*K*). Furthermore,
15 increased expression of *YAP1-2α* and elevated formation of nuclear YAP1
16 condensates were correlated with advanced clinical stages (Fig. 6*O*, Fig.
17 S6*L*). In this regard, although total YAP1 expression in HGSOC tissue was
18 significantly higher than that in normal ovarian tissue, no significant
19 correlation was observed between YAP1 expression levels and clinical
20 stages in HGOC patients (Fig. 6*P*). This indicated that HGSOC progression
21 is not due to elevated YAP1 expression, but is associated with splice
22 switching of *YAP1* pre-mRNA leading to accumulation of YAP1-2α. These
23 findings suggested that YAP1-2α, the specific YAP1 isoform, enhances the

robustness and resilience of HGSOC cells by altering transcriptional networks through LLPS (formation of nuclear condensates), thereby promoting the acquisition of more malignant phenotypes that accelerate cancer progression.

Relationship between the YAP1-2α isoform and anti-cancer drug resistance

YAP1-2α accelerates cellular phenotypes associated with neoplastic transformation. However, it remains unclear which cellular conditions influence the splicing patterns of *YAP1* pre-mRNA. Because LLPS-mediated YAP1-2α puncta formation reduces sensitivity to genotoxic drugs such as Cisplatin (Fig.6K), we hypothesized that a splicing switch in *YAP1* pre-mRNA occurs during the acquisition of Cisplatin resistance. To investigate the relationship between the *YAP1* pre-mRNA splicing switch and drug resistance, we established ten independent Cisplatin-resistant clones from UWB1.289 cells after three months of culture with stepwise increases (100 pM to 100 nM) in Cisplatin concentration. Analysis of the *YAP1* pre-mRNA splicing pattern in those clones, using PCR that specifically detects inclusions and exclusions in exon 6 (19), revealed that several Cisplatin-resistant clones exhibited changes in *YAP1* isoforms compared to the parental UWB1.289 cells. However, some clones also exhibited Cisplatin resistance without changes in *YAP1* mRNA splicing patterns (Fig. 7*A*, Fig. S7*A*). To examine the impact of the splicing switch in *YAP1* pre-mRNA on the acquisition of Cisplatin resistance, we

1 arbitrarily selected two clones (R2 and R3), in which Exon 6 was excluded
2 from most *YAP1* mRNAs, and one clone (R5) that did not show significant
3 changes in the splicing patterns of *YAP1* mRNA. Using these cell clones,
4 we tested the necessity of the YAP1-TEAD complex for Cisplatin
5 sensitivity. Treatment with K-975, a specific YAP1-TEAD inhibitor,
6 significantly restored Cisplatin sensitivity in R2 and R3 clone cells, but
7 not in R5 clone cells (Fig. S7*B*). Inhibiting YAP1 expression in R2 and R3
8 cell clones using shRNA targeting the entire *YAP1* mRNA restored
9 Cisplatin resistance, which was counteracted by ectopic co-expression of
10 shRNA-resistant YAP1-2α, but not YAP1-2γ (Fig. 7, *B*-*C*, Fig. S7*C*). Since
11 YAP1 LLPS-induced nuclear puncta are associated with the formation of
12 the YAP1-2α/TAZ/TEAD super-enhancer, we next examined whether
13 YAP1 puncta formation is linked to the splicing switch of *YAP1* pre-mRNA
14 in Cisplatin-resistant R2 and R3 cells. Immunofluorescence analysis
15 revealed the formation of YAP1 puncta in those cells. TAZ also colocalized
16 with these puncta. In contrast, such colocalization was not observed in
17 parental cells or in R5 cells (Fig. 7, *D*-*E*). The formation of endogenous
18 YAP1-2α/TAZ/TEAD complexes was also significantly higher in R2 cells
19 than in parental cells (Fig. 7*F*). Knockout of *TAZ* in the Cisplatin-resistant
20 R2 clone impaired YAP1 puncta formation (Fig. 7, *G*-*H*, Fig. S7*D*) and
21 increased Cisplatin sensitivity (Fig. 7*I*). In contrast, ectopic
22 overexpression of TAZ in parental UWB1.289 cells did not alter Cisplatin
23 susceptibility (Fig. 7*J*, Fig. S7*E*). JQ1, a selective inhibitor of BRD4-
24 regulated super-enhancers, restored Cisplatin sensitivity in Cisplatin-

1 resistant clones R2 and R3, but not in R5 (Fig. S7*F*). These results
2 collectively indicated that, while YAP1-independent mechanisms certainly
3 exist, the YAP1-2α/TAZ/TEAD super-enhancer generated by the splicing
4 switch of *YAP1* mRNA from *YAP1-2γ* (inclusion of Exon 6) to *YAP1-2α*
5 (exclusion of Exon 6) is one of the mechanisms that underpin the
6 acquisition of tumor cell resistance to anti-cancer drugs.
7

Discussion

This study demonstrated that YAP1-2α, a specific YAP1 isoform, induces LLPS-mediated nuclear biomolecular condensates that activate TEAD-positive super-enhancers, inducing EMT-related genes that strengthen the malignant phenotype of cancer cells. In fact, elevated levels of YAP1-2α expression correlate with poor prognosis in HGSOC. YAP1-2α heterodimerizes with TAZ via the leucine zipper without influencing YAP1-2α/TEAD and TAZ/TEAD complex formation. The YAP1-2α/TAZ heterodimerization then induces LLPS that generates nuclear condensates by provoking multivalent interactions between the three WW domains in the YAP1-2α/TAZ heterodimer and the PPxY/LPxY WW domain-binding motifs present in multiple numbers in BRD4, which in turn activate YAP1-2α/TAZ/TEAD-specific super-enhancers. YAP1-1α can also heterodimerize with TAZ through the leucine zipper. However, YAP1-1α hardly induces puncta formation, presumably because of its single WW domain, which cannot mediate multivalent protein-protein interactions underlying LLPS induction. Independent of YAP1, TAZ promotes LLPS-mediated puncta formation via leucine zipper-mediated TAZ/TAZ homodimerization. In contrast to TAZ, YAP1-1α and YAP1-2α cannot homodimerize or heterodimerize, owing to the structural incompatibilities between identical leucine zipper sequences (19, 33, 58). TAZ is, therefore, capable of forming a minimum of two distinct super-enhancers, one involving the YAP1-2α/TAZ heterodimer and the other involving the

TAZ/TAZ homodimer, each of which may regulate different sets of target genes.

YAP1 and TAZ regulate numerous genes, including those involved in cell proliferation, cell-cell contact, cell polarity, cellular stress, cell metabolism, and cell cycle (7-13). Despite their redundant roles in gene regulation, as their primary partner transcription factors are TEADs (TEAD1-4), most studies have suggested that the YAP1/TEAD and TAZ/TEAD transcriptional complexes function independently (58, 59). Among the eight YAP1 isoforms present in human cells by differential splicing of *YAP1* pre-mRNA (14, 15), YAP1-2γ and YAP1-2δ, which lack a functional leucine zipper, are abundantly expressed in normal and cancer cells. Consequently, our understanding of the YAP1/TAZ heterodimer was very limited until the discovery that the minor YAP1 isoforms, YAP1-1α and YAP1-2α, can bind TAZ via leucine zippers (19). The present study further revealed that YAP1-2α/TAZ heterodimerization specifically activates EMT-related genes, contributing to elevated malignant traits in cancer cells. Indeed, a comprehensive analysis of YAP1 splicing isoforms reported that YAP1-2α also shows distinct transcriptional regulation compared to other isoforms and is responsible for higher transcriptional activity of typical TEAD target genes (16). The study strongly supports our conclusion that YAP1-2α promotes nuclear puncta formation and enhances transcriptional activity distinct from other isoforms. Additionally, NIH3T3 cells expressing YAP1-2α was shown to exhibit

higher tumorigenicity *in vivo* compared to NIH3T3 cells expressing YAP1-2γ (19). Therefore, increased YAP1-2α expression plays a crucial role in the elevated *in vivo* tumorigenesis.

Several studies have reported findings regarding YAP1-containing LLPS. IFN-γ induced by sustained treatment with anti-PD-1 immunotherapy promoted formation of YAP1 LLPS in a YAP1 leucine zipper-dependent manner, which induces resistance to the treatment via elevation of key immunosuppressive target gene expression (60). Hyperosmotic stress, which promotes YAP1 LLPS, including TEAD and TAZ, alters transcriptional capacity by activating super-enhancers (61). In the present study, we discovered that YAP1-2α, a specific YAP1 splicing isoform, is essential for the efficient formation of YAP1 LLPS. Since only YAP1-1α and YAP1-2α possess a functional leucine zipper and bind to TAZ, the splicing switch of *YAP1* pre-mRNA may play a pivotal role in YAP1-LLPS formation. Although the regulatory mechanisms of *YAP1* alternative splicing remain largely unclear, it has been reported that the neonatal alternative splicing program is rewired in damaged regenerating hepatocytes to activate the Hippo-YAP1 signaling pathway (62). During this process, the YAP1 splicing switch is induced, leading to increased expression of YAP1-2α, implying that changes in the microenvironment associated with chronic tissue damage caused by inflammation and other factors may rewire splicing mechanisms and induce splicing abnormalities in genes involved in cancer progression, including YAP1.

YAP1 activates cytokines and chemokines, thereby promoting the

1 polarization and recruitment of myeloid-derived suppressor cells
2 (MDSCs) and tumor-associated macrophages (TAMs), which subsequently
3 inactivate T cells (63, 64). Indeed, TCGA HGSOC cohort indicated that
4 *YAP1-α*^{dominant} cancers exhibit elevated inflammatory response signaling.
5 Also, it has been reported that interferon-γ induces leucine zipper motif-
6 dependent phase separation of YAP1, which activates target genes
7 involved in immunosuppression (60). This activation may be mediated by
8 YAP1/TAZ/TEAD super-enhancers, thereby facilitating immune evasion
9 by cancer cells. YAP1-2α/TAZ/TEAD LLPS-mediated gene regulation may
10 therefore augment cell-intrinsic robustness while creating cell-extrinsic
11 conditions that foster cancer cells, establishing a "cold" immune
12 environment that contributes to the malignant progression of cancer.
13 The present study elucidated an unanticipated molecular connection
14 between alternative mRNA splicing (splice-switching), liquid-liquid phase
15 separation (LLPS), and gene regulations, which significantly alters cancer
16 cell characteristics without genetic mutations. Recent studies have
17 indicated an intimate correlation between aberrant alternative splicing and
18 cancer (2). The findings of this study provide valuable insights into the
19 mechanisms by which splicing abnormalities contribute to cancer
20 progression. Activating YAP1-2α/TAZ/TEAD LLPS confers a more
21 aggressive and malignant phenotype. In turn, the finding indicates
22 selective inhibition of differential splicing that generates YAP1-2α mRNA
23 or specific disruption of YAP1-2α/TAZ/TEAD-induced LLPS impedes

cancer progression.

There are several limitations in these studies. For instance, the RNA-seq analysis was conducted using the public database for human HGSOC patients (Fig. 5, *A*-*B*, Fig. S5*A*), and the expression of *YAP1* isoforms was defined based on PSI. Consequently, it was not possible to analyze the actual protein expression levels of each YAP1 isoform in these studies. Another limitation also existed regarding the types of cancer. In our study, two cell lines (ovarian cancer, UWB1.289, and breast cancer, MDA-MB-436) were used to eliminate the influence of cell line type when analyzing the molecular mechanisms underlying YAP1 LLPS formation. However, these cells have specific genetic backgrounds, including *BRCA1* mutations that increase sensitivity to Cisplatin due to a deficiency in homologous recombination (65). Hence, further research is needed to determine whether the switch in splicing isoform of *YAP1* mRNAs from YAP1-2γ to YAP1-2α confers drug resistance beyond cisplatin in cancers that do not carry the *BRCA1* mutations. It should be interesting to determine whether there is an association between YAP1 splicing patterns and the malignant grades of tumors by analyzing differences in tumorigenic phenotypes, such as those between the basal-like and classical subtypes of pancreatic cancer (66) and between the diffuse and intestinal types of gastric cancer (67).

Experimental procedures

Cell Lines

UWB1.289 cells (ATCC, CRL-2945) were cultured in 1:1 mixed medium supplemented with 3% FBS (Gibco), a 1:1 mixture of mammary epithelial cell growth medium (MEGM) (Lonza, CC-3150) without GA-1000 (gentamicin-amphotericin B mixture) and RPMI-1640 (Wako, 189-02025) supplemented with 10 mM HEPES and 1 mM sodium pyruvate. MDA-MB-436 (ATCC, HTB-130) cells were cultured in RPMI-1640 supplemented with 10% FBS (Gibco), 10 mM HEPES, and 1 mM sodium pyruvate. Lenti-X 293T cells (Clontech Laboratories, 632180) were cultured in D-MEM (Wako, 044-29765) supplemented with 10% FBS (Gibco) and 1 mM sodium pyruvate. Cells were incubated at 37 °C in 5% CO_2.

To generate gene knockout (KO) cell lines, cells were transfected with pX330-sgYAP1 or pX330-sgTAZ vector and a blasticidin S or puromycin resistance gene. After transfection, the cells were selected using blasticidin S (10 μg/ml), or puromycin (1 μg/ml) and cloned by limiting dilution.

Three-Dimensional Overlay Culture

UWB1.289 cells were suspended in 1:1 mixed medium containing 2% Matrigel (CORNING, #356231) (termed assay medium) and seeded onto Matrigel in 8-well chamber slides at 4×10^3 cells/well. Eight days after seeding, the spheroids were treated with 100 nM JQ1 (MedChemExpress, HY-13030), 1 μM K-975 (MedChemExpress, HY-138565), or DMSO as a mock control for 6 days. During cultivation, the assay medium with or without the indicated reagent was replaced every two days. After treatment with the appropriate reagents, spheroids were fixed with 2% paraformaldehyde for 20 min and collected using a cell-recovery solution (CORNING, 354253). The fixed spheroids were permeabilized with 0.5% TritonX-100 in PBS for 20 min at room temperature and subjected to

immunostaining analysis. The Ferret diameters of spheroids were analyzed by measuring images captured 14 days after seeding using the ImageJ software.

Expression Vectors

Base substitution and deletion mutants were generated using a KOD-plus-Mutagenesis kit according to the manufacturer's instructions (TOYOBO, SMK-101). Nucleotide sequences of all constructed vectors were confirmed by Sanger sequencing. See supporting information for RNAi and sgRNA target sequences.

Preparation of Lentivirus and Infections

The lentivirus was produced according to our previous protocol (68).

Live Cell Imaging

Cells transfected with mVenus-fused YAP1 isoforms were subjected to analysis to confirm the liquid-like properties (fusion event of puncta, disruption of puncta formation by treatment with Hex and FRAP). To detect the fusion event of the YAP1-2α puncta, time-lapse fluorescence images of cells transfected with mVenus-fused YAP1-2α were obtained for 120 s using a FLUOVIEW FV1200 confocal microscope (Olympus). To observe the disruption of YAP1-2α puncta formation by Hex treatment, transfected cells were treated with 1% Hex for 20 min. Twenty minutes after Hex treatment, the cells were washed and incubated for another 4 h. Fluorescence signals were detected at the indicated time points.

Fluorescence Recovery After Photobleaching (FRAP)

The mVenus-fused YAP1-2α nuclear puncta specified by the ROI were photobleached by laser irradiation. After photobleaching, time-lapse fluorescence images of the YAP1-2α puncta were obtained for 120 sec. Unbleached puncta were used as controls. The images were acquired at 3.2

second intervals using a 40x objective lens. The fluorescence intensities of puncta obtained from a series of time-lapse images were analyzed using FLUOVIEW FV1200 software. The fitting equation for determining the diffusion coefficient "*D*" is shown below

$D = (0.88 \cdot r^2)/4t_{1/2}$

r: radius of the bleached area

$t_{1/2}$: half-time of recovery

Immunofluorescence Staining

Cells were fixed with 2% or 4% paraformaldehyde in PBS for 15 min at room temperature or 37°C, permeabilized with 0.25% TritonX-100 in PBS for 10 min at room temperature, and blocked in blocking solution (5% BSA, 0.1% Tween20, 0.05% NaN3 in PBS) for 60 min at room temperature. For spheroid staining, fixed and collected spheroids were permeabilized with 0.5% TritonX-100 in PBS for 20 min at room temperature. Blocked cells/spheroids were incubated with primary antibodies against YAP1 (CST, 12395, lot 3, 1:500; CST, 14074, lot 5, 1:500), HA-tag (CST, 2367, lot 5, 1:500 or CST, 3724, lot 13, 1:500), TAZ (CST, 83669, lot 2, 1:500), pan-TEAD (CST, 13295, lot 2, 1:500), Flag-tag (SIGMA, F3165, lot SLCP4941, 1:1000), BRD4 (CST, 13440, lot 9, 1:500), ki67 (Thermo Fisher Scientific, 14-5698-80, lot 2047169, 1:500), or Pol II (Santa Cruz Biotechnology, sc-47701, lot 1123, 1:500). After the antigen-antibody reaction, Alexa Fluor-conjugated secondary antibodies (1:1000) and/or Alexa Fluor-conjugated phalloidin (Invitrogen) were used. Nuclei were stained with DAPI (wako, 043-18804, 1:1000) solution or DRAQ5 (CST, 4083, 1:1000). The number of YAP1 puncta was calculated using ImageJ. The parameters used to identify the puncta are as follows.

Image > Type > 16-bit; Adjust > Threshold > 50-65535

Analyze > Analyze particles > size (0.1-100), circularity (0.3-1.0)

The intensity of YAP1 nuclear expression in individual cells was measured using ImageJ. Regions of interest (ROIs) were defined based on DAPI or

DRAQ5 staining. The parameters used to identify the ROI are as follows.

Image > Type > 16-bit, Adjust > Threshold > 50-65535

Analyze > Analyze particles > size (20-infinity), circularity (0.2-1.0)

Proximity Ligation Assay (PLA)

PLA was performed using a Duolink *In situ* PLA kit (SIGMA, Duo92007, Duo92002, Duo92004) according to the manufacturer's instructions. For more details on PLA analysis, see our published protocol (68).

Immunohistochemistry

The human ovarian cancer tissue arrays (OV0071a, OV1004A, US Biomax) were deparaffinized and rehydrated. Antigen retrieval was performed by boiling for 15 minutes in 1x Target Retrieval (ACD). To block endogenous peroxidase activity, the tissue array was incubated with 3% hydrogen peroxide in double-distilled water for 10 min at room temperature. The array was then incubated overnight at 4 °C with a primary antibody against YAP1 (CST, 14074, lot 5, 1:400). After the antigen-antibody reaction, the array was incubated for 60 min at room temperature with Alexa Fluor-conjugated secondary antibodies (1:1000). After the secondary antibody reaction, the nuclei were stained with DAPI solution (1:1000) for 20 min at room temperature. Fluorescence images were obtained using the FLUOVIEW FV1200 confocal microscope. H&E staining was performed using the Hematoxylin and Eosin Stain kit (ScyTek Laboratories).

In Situ Hybridization (BaseScope)

Deparaffinized and rehydrated tissue arrays were subjected to *in situ* hybridization (BaseScope). BaseScope was performed using the BaseScope Detection Reagent Kit v2-RED (ACD) according to the manufacturer's instructions. The human YAP1-1/2α-isoform-specific probe (BA-Hs-YAP1-tv3-E5E6) was designed using an ACD. The

expression levels of *YAP1-2α* mRNA were determined by measuring the *YAP1-2α* mRNA BaseScope signals using the ImageJ software. *YAP1-2α* mRNA expression was scored as 0: no staining or less than 1 dot to every 20 cells; 1+: 1 dot/cell; 2+: 2-3 dots/cell, no or very few dot clusters; 3+: 4-10 dots/cell, less than 10% positive cells have dot clusters; 4+: >10 dots/cell, more than 10% positive cells have dot clusters. Staining scores were set according to the scoring guidelines of BaseScope.

Induction of Artificial Heterodimer Complexes

To induce artificial heterodimerization between YAP1-2α(LZM) and TAZ(LZM) or YAP1-2γ/TAZ(LZM), we constructed expression vectors for DmrC-mSECFP-fused 3xFlag-YAP1-2α(LZM), DmrC-mSECFP-fused 3xFlag-YAP1-2γ, and DmrA-mVenus-fused HA-TAZ(LZM). These vectors were transiently transfected into UWB1.289 cells. The cells were then cultured for 24 h, treated with the A/C heterodimerizer (Clontech, Z5057N), and subjected to immunoprecipitation, fluorescence imaging analysis, and qPCR analysis. Ethanol (EtOH) was used as a mock control

To induce a stable heterodimer between YAP1-2α(S127A-LZM)-WW1/2^{WT} and TAZ(LZM) or between YAP1-2α(S127A-LZM)-WW1/2^{mut} and TAZ(LZM) in cells, we generated lentiviruses that transduce DmrC-mSECFP-fused 3xFlag-YAP1-2α(S127A-LZM)-WW1/2^{WT} and DmrC-mSECFP-fused 3xFlag-YAP1-2α(S127A-LZM)-WW1/2^{mut}. UWB1.289-derived (cloned) cells expressing DmrA-mVenus-fused HA-TAZ(LZM) were then infected with these lentiviruses. Cells transduced with the indicated lentiviruses were selected with puromycin for 7 days. The resulting cells were treated with the A/C heterodimerizer and analyzed for changes in oncogenic properties.

Immunoprecipitation and Immunoblotting

The cells were washed in ice-cold PBS and lysed in lysis buffer (100 mM NaCl, 50 mM Tris-HCl pH 7.5, 5 mM EDTA, 2 mM Na_3VO_4, 10 mM

NaF, 10 mM β-glycerophosphate, 2 mM PMSF, 10 μg/ml leupeptin, 10 μg/ml trypsin inhibitor, 10 μg/ml aprotinin, and 0.4% NP-40). Cell lysates were incubated with protein G-beads after incubation with anti-TAZ (CST, 83669, lot 2, 1:500), anti-HA (CST, 3724, lot 13, 1:500), anti-Flag (SIGMA, F3165, lot SLCP4941, 1:1000), anti-YAP1 (CST, 14074, lot 5, 1:500), or isotype control IgG. The beads were washed five times with lysis buffer, and the immunoprecipitates were eluted with SDS sample buffer. The immunoprecipitates and total cell lysates were subjected to SDS-PAGE and then immunoblotted. Images were captured using the LAS-4000 imager (FUJIFILM). To compare protein expression levels, protein band intensities from three biological replicates were collected and quantitatively analyzed using the LAS-4000 luminoimage analyzer (FUJIFILM). Exposure time for detection was automatically calculated to stay within the LAS-4000 dynamic range, and signal linearity was maintained within this range.

Chromatin immunoprecipitation

To evaluate interaction between genome DNA and target proteins, DNA samples were prepared using the CUT & RUN and the ChIP-re-chip. CUT & RUN was performed using CUT & RUN Assay Kit (CST) according to the manufacturer's instructions, employing anti-BRD4 (CST, 13440, lot 9, 1:50), anti-HA (CST, 3724, lot 13, 1:50), anti-TAZ (CST, 83669, lot 2, 1:50), or anti-panTEAD (CST, 13295, lot 2, 1:50) antibody. Rabbit IgG (CST, 66362, lot 3, 1: 20) was used as the isotype control. For ChIP-re-chip, *YAP1*-KO UWB1.289 cells were transfected with 6xHis-tagged YAP1-2α and treated with K-975 or DMSO. Twenty-four hours after K-975 treatment, a cross-linking reaction with formaldehyde (CST, 12606) was performed, followed by chromatin isolation and sonication. Cross-linked chromatin was pulled down using Ni Sepharose excel (Cytiva) and eluted with 500 mM imidazole. The imidazole was replaced with a lysis buffer by centrifugal ultrafiltration (Millipore, UFC903024), and immunoprecipitation was performed using anti-TAZ antibody (CST, 83669,

lot 2) or rabbit IgG (CST, 66362, lot 3) as an isotype control. Chromatin bound to YAP1-2α/TAZ complex was reversed and the DNA fragments were purified using spin columns (CST, 14209). Purified DNA samples were subjected to PCR or qPCR analysis.

Quantitative PCR (qPCR)

Total RNA was extracted from cells using TRIzol reagent (Invitrogen) and reverse-transcribed using the High-Capacity cDNA Reverse Transcription Kit (Thermo Fisher Scientific, 4368814). Relative mRNA expression was analyzed using the QuantStudio 3 Real-Time PCR System (Thermo Fisher Scientific) with SYBR *Premix Ex Taq* Tli RNaseH Plus (TaKaRa). *18S* rRNA was used as an internal control. The data were analyzed using the comparative CT (ΔΔCT) method. For ChIP-qPCR analysis, purified DNA fragments prepared by CUT & RUN and ChIP-re-chip were analyzed using the QuantStudio 3 Real-Time PCR System with KOD-SYBR qPCR Mix (TOYOBO). See supporting information for primer sequences.

Detection of YAP1 Splicing Isoforms

Total RNA was extracted from the cells using TRIzol reagent (Invitrogen, 15596026) and reverse-transcribed using oligo(dT) primers and SuperScript II Reverse Transcriptase (Invitrogen, 18064014). The resulting cDNA was subjected to PCR to detect the YAP1 exon 6 sequence, which encodes the γ-segment. After PCR, the amplicon was loaded onto a 2% TAE-agarose gel and electrophoresed.

Luciferase Reporter Assay

A luciferase reporter assay was performed using a dual luciferase reporter assay kit (Promega). See our previous work for details (68). To examine the effect of YAP1-2α mutants on TEAD activity, *YAP1*-KO UWB1.289 cells were transfected with the TEAD reporter plasmid together

with the indicated mVenus-fused YAP1-2α mutant expression vector (wild-type, LZM, S94A, LZM|S94A) using Lipofectamine 2000 reagent (Invitrogen), and 48 h after transfection, cells were collected using passive lysis buffer (Promega). Luminescence was detected using a Centro XS^3 LB960 (BERTHOLD). The relative luciferase activities were calculated as fold changes relative to the values of the control samples. To confirm the protein expression levels of the mVenus-fused YAP1-2α mutants, the remaining cell lysates were subjected to immunoblotting.

Cell Viability Assay

Sensitivity to anti-cancer agents and 2D cell proliferation was measured by MTS assay using CellTiter 96 AQueous One Solution Cell Proliferation Assay (Promega, G3580) according to the manufacturer's instructions. To examine drug sensitivity, 1,000 cells were seeded into each well of 96-well plates and treated with stepwise concentrations of anticancer agents (Cisplatin, Sorafenib, Trametinib) for 72 h. To examine sensitivity to Olaparib, 500 cells were seeded into each well of 96-well plates and treated with a stepwise concentration of Olaparib for 6 days. After treatment with anti-cancer agents, the cells were incubated with the MTS assay reagent at 37 °C in 5% CO_2. After 60-90 min of incubation, the absorbance at 490 nm was measured using Multiskan FC (Thermo Fisher Scientific). The relative cell viability was calculated using mock-treated cells. In experiments designed to examine the effects of JQ1 or K-975, cells were treated with 100 nM JQ1, 1 μM K-975, or DMSO as a mock control for 3 days, then seeded into a 96-well plate.

Three-dimensional Cell Viability Assay

To examine anchorage-independent growth, cells were seeded at 500 cells per well into an Ultra-Low Attachment 96-well plate (CORNING) and cultured for 12 days. During cultivation, the medium was replaced every 2 days. Appropriately cultured spheroids were lysed in CellTiter-

Glo 3D Cell Viability Assay Reagent (Promega, G9683). The 200 μl cell lysate obtained from each well was immediately transferred into a white 96-well plate (Greiner) and luminescence was measured using Centro XS^3 LB960. To ensure linearity of the luminescence signal in these assays, dilution operations were performed as appropriate.

Ferroptosis Assay

Cells treated with 100 nM JQ1, 1 μM K-975, or DMSO as a mock control for 3 days were seeded into a 96-well plate (Greiner) and further treated with chlorido [N, N'-Disalicylidene-1,2-Phenylenediamine] Iron (III) (Cayman Chemical Company, 28788) or DMSO as a mock control for 48 h. Cultured cells were lysed in CellTiter-Glo 3D Cell Viability Assay reagents (Promega). Cell viability was determined by detecting luminescence using a Centro XS3 LB960.

Migration and Invasion Assay

Cells treated with 100 nM JQ1, 1 μM K-975, or DMSO as a mock control for 3 days were seeded into Transwell (Costar: 3464) inserted into 24-well plates (Coster: 3526). Transwell coated with type-I-A collagen gel (Wako), prepared according to the manufacturer's protocols, was used to examine the ability of the cells to infiltrate the extracellular matrix (invasion assay). The cells were further cultured in medium containing 0.1% FBS for 48 h (chemotaxis assay) or 2 weeks (invasion assay). The bottom wells were filled with medium containing 10% FBS. After incubation for the appropriate time, cells that had migrated or infiltrated into the lower wells were lysed in CellTiter-Glo 3D Cell Viability Assay regents. The cell number was determined by detecting luminescence using Centro XS3 LB960.

Analysis of HGSOC RNA-seq Data

PSI [percent spliced in index: the ratio of normalized read counts

indicating inclusion of a transcript element over the total normalized reads for that event (both inclusion and exclusion reads)] data for the *YAP1* mRNA splicing variants containing γ-segment (referred to as *YAP1-E6*) and *YAP1* mRNA splicing variants containing β-segment (referred to as *YAP1-E5.2*) were downloaded directly from the TCGA SpliceSeq (https://bioinformatics.mdan derson.org/TCGASpliceSeq/singlegene.jsp) (46). HGSOC RNA-seq data was downloaded directly from the cBioportal for Cancer Genomics (https://www.cbioportal.org/) (43-45). For subgrouping the TCGA cohorts, expression of *YAP1* isoforms were defined as "*YAP1-*$\alpha^{dominant}$" [PSI (*YAP1-exon 6*) < median, PSI (*YAP1-exon 5.2*) < median], "*YAP1-*$\beta^{dominant}$" [PSI (*YAP1-exon 6*) < median, PSI (*YAP1-exon 5.2*) > median], "*YAP1-*$\gamma^{dominant}$" [PSI (*YAP1-exon 6*) > median, PSI (*YAP1-exon 5.2*) < median], or "*YAP1-*$\delta^{dominant}$" [PSI (*YAP1-exon 6*) > median, PSI (*YAP1-exon 5.2*) > median]. HGSOC patients (n = 425) were divided into the "*YAP1-*$\alpha^{dominant}$" (n = 131), "*YAP1-*$\beta^{dominant}$" (n = 83), "*YAP1-*$\gamma^{dominant}$" (n = 78), and "*YAP1-*$\delta^{dominant}$" (n = 133). TPM count for "*YAP1-*$\alpha^{dominant}$" and "*YAP1-*$\gamma^{dominant}$" were analyzed using iDEP v2.4.0 web tool (https://bioinformatics.sdstate.edu/idep/) (69) to perform DEG analysis. Genes whose expression increased in "*YAP1-*$\alpha^{dominant}$" vs. "*YAP1-*$\gamma^{dominant}$" (FDR < 0.1, FC >1.5) were further subjected to gene enrichment analysis (Hallmark MSigDB) using the gene-set enrichment tool ShinyGO (https://bioinformatics.sdstate.edu/go/) (70).

Prediction of SE elements

Identified super-enhancer elements in serous ovarian cancer cells (GSM3328052: PEO1) (40) and triple-negative breast cancer cells (GSM6132824: MDA-MB-436) (41) were downloaded from SEdb3.0 (http://www.licpathway.net/sedb). TEAD1 and TEAD4-binding motif elements were downloaded from JASPR (https://jaspar.elixir.no/) (71). The downloaded data were visualized using IGV (https://igv.org/app/).

Statistical analysis

The specific statistical methods used are indicated in the figure legends and were calculated using Microsoft Excel and PRISM GraphPad software. Unpaired T-tests (Student's T-test and Welch's T-test) and U-tests were performed to compare the two groups. Details of the analysis are provided in the respective methods. All experiments presented in the manuscript were repeated in technical or biological replicates.

Data availability

All the other data supporting the findings of this study are available within the article and its supplementary information files. This study did not generate the original code.

Supporting information – This article contains supporting information.

Acknowledgments – We thank Dr. Naoko Murata-Kamia for valuable discussions. This work was partly supported by the Microbial Chemistry Research and Development Grant, funded by grant number 23A02 from the Microbial Chemistry Research Foundation.

Author contributions – T.O. and M.H. conceptualization; T.O. and T.H. methodology; T.O., T.H., and Y.Y. formal analysis; T.O., T.H., and Y.Y. investigation; T.O. and M.H. writing-original draft; T.O., T.H., and M.H. writing-review & editing; M.H. supervision; M.H. project administration.

Funding and additional information - This work was supported by a JSPS Grant-in-Aid for Scientific Research from the Japan Society for the Promotion of Science Grant numbers 21H04804 (M.H.) 24H00618 (M.H.), and JP21K15526 (T.O.), P-PROMOTE from AMED Grant Number JP23ama221219h0001 (M.H.) Further information and requests should be addressed to Masanori Hatakeyama (mhata@m.u-tokyo.ac.jp).

Conflict of interest

The authors declare that they have no conflicts of interest with the contents of this article.

Abbreviations - The abbreviations used are: YAP1, yes-associated protein 1; TAZ, transcriptional coactivator with PDZ-binding motif; TEAD, TEA domain transcription factor; BRD4, bromodomain containing 4; LLPS, liquid-liquid phase separation; SPARC, secreted protein acidic and cysteine rich; ALDH1A3, aldehyde dehydrogenase 1 family member A3; EMT, epithelial-mesenchymal transition; HGSOC, high-grade serous ovarian cancer.

References

1. Oltean, S., and Bates, D.O. (2014) Hallmarks of alternative splicing in cancer. *Oncogene*. **33**, 5311-5318
2. Bradley, R.K., and Anczuków, O. (2023) RNA splicing dysregulation and the hallmarks of cancer. *Nat Rev Cancer*. **23**, 135-155
3. Peng, Q., Zhou, Y., Oyang, L., Wu, N., Tang, Y., Su, M., Luo, X., Wang, Y., Sheng, X., Ma, J., and Liao, Q. (2022) Impacts and mechanisms of alternative mRNA splicing in cancer metabolism, immune response, and therapeutics. *Mol Ther*. **30**, 1018-1035
4. Zhao, B., Ye, X., Yu, J., Li, L., Li, W., Li, S., Yu, J., Lin, J.D., Wang, C.Y., Chinnaiyan, A.M., et al. (2008) TEAD mediates YAP-dependent gene induction and growth control. *Genes Dev*. **22**, 1962-1971
5. Zhang, H., Liu, C.Y., Zha, Z.Y., Zhao, B., Yao, J., Zhao, S., Xiong, Y., Lei, Q.Y., and Guan, K.L. (2009) TEAD transcription factors mediate the function of TAZ in cell growth and epithelial-mesenchymal transition. *J. Biol. Chem*. **284**, 13355-13362
6. Zanconato, F., Battilana, G., Forcato, M., Filippi, L., Azzolin, L., Manfrin, A., Quaranta, E., Di, Biagio. D., Sigismondo, G., Guzzardo, V., et al. (2018) Transcriptional addiction in cancer cells is mediated by YAP/TAZ through BRD4. *Nat Med*. **24**, 1599-1610
7. Zheng, Y., and Pan, D. (2019) The Hippo signaling pathway in development and disease. *Dev. Cell*. **50**, 264-282
8. Thrash, H.L., and Pendergast, A.M. (2023) Multi-functional regulation by YAP/TAZ signaling networks in tumor progression and metastasis. *Cancers*. **15**, 4701
9. Kim, M.H., and Kim, J. (2017) Role of YAP/TAZ transcriptional regulators in resistance to anti-cancer therapies. *Cell. Mol. Life Sci*. **74**, 1457-1474
10. Shao, D.D., Xue, W., Krall, E.B., Bhutkar, A., Piccioni, F., Wang, X., Schinzel, A.C., Sood, S., Rosenbluh, J., Kim, J.W., et al. (2014) KRAS and YAP1 converge to regulate EMT and tumor survival. *Cell*. **158**, 171-184

11. Lin, L., Sabnis, A.J., Chan, E., Olivas, V., Cade, L., Pazarentzos, E., Asthana, S., Neel, D., Yan, J.J., Lu, X., et al. (2015) The Hippo effector YAP promotes resistance to RAF- and MEK-targeted cancer therapies. *Nat. Genet*. **47**, 250-256
12. Zanconato, F., Forcato, M., Battilana, G., Azzolin, L., Quaranta, E., Bodega, B., Rosato, A., Bicciato, S., Cordenonsi, M., and Piccolo, S. (2015) Genome-wide association between YAP/TAZ/TEAD and AP-1 at enhancers drives oncogenic growth. *Nat. Cell Biol.* **17**, 1218-1227
13. He, L., Pratt, H., Gao, M., Wei, F., Weng, Z., and Struhl, K. (2021) YAP and TAZ are transcriptional coactivators of AP-1 proteins and STAT3 during breast cellular transformation. *Elife*. **10**, e67312
14. Gaffney, C.J., Oka, T., Mazack, V., Hilman, D., Gat, U., Muramatsu, T., Inazawa, J., Golden, A., Carey, D.J., Farooq, A., et al. (2012) Identification, basic characterization and evolutionary analysis of differentially spliced mRNA isoforms of human YAP1 gene. *Gene*. **509**, 215-222
15. Sudol, M. (2013) YAP1 oncogene and its eight isoforms. *Oncogene*. **32**, 3922
16. Vrbský, J., Vinarský, V., Perestrelo, A.R., De La Cruz, J.O., Martino, F., Pompeiano, A., Izzi, V., Hlinomaz, O., Rotrekl, V., Sudol, M., Pagliari, S., and Forte, G. (2021) Evidence for discrete modes of YAP1 signaling via mRNA splice isoforms in development and diseases. *Genomics*. **113**, 1349-1365
17. Ingham, R.J., Colwill, K., Howard, C., Dettwiler, S., Lim, C.S.H., Yu, J., Hersi, K., Raaijmakers, J., Gish, G., Mbamalu, G., et al. (2005) WW domains provide a platform for the assembly of multiprotein networks. *Mol. Cell. Biol*. **25**, 7092-7106
18. Yang, Y., Wu, M., Pan, Y., Hua, Y., He, X., Li, X., Wang, J., and Gan, X. (2024) WW domains form a folded type of nuclear localization signal to guide YAP1 nuclear import. *J Cell Biol*. **223**, e202308013
19. Ben, C., Takahashi-Kanemitsu, A., Wu, X., Knight, C.K., and Hatakeyama, M. (2020) Alternative splicing reverses the cell-intrinsic and cell-extrinsic

prooncogenic potentials of YAP1 via SHP2. *J. Biol. Chem.* **295**, 13965-13980

20. Huang, Z., Liu, Z., Chen, L., Liu, Y., Yan, G., Ni, Y., Yan, Q., He, W., Liu, J., Luo, S., and Xie, J. (2025) Liquid-liquid phase separation in cell physiology and cancer biology: recent advances and therapeutic implications. *Front Oncol.* **15**, 1540427
21. Wang, B., Zhang, L., Dai, T., Qin, Z., Lu, H., Zhang, L., and Zhou, F. (2021) Liquid-liquid phase separation in human health and diseases. *Signal Transduct Target Ther.* **6**, 290
22. Sabari, B.R., Dall'Agnese, A., Boija, A., Klein, I.A., Coffey, E.L., Shrinivas, K., Abraham, B.J., Hannett, N.M., Zamudio, A.V., Manteiga, J.C., et al. (2018) Coactivator condensation at super-enhancers links phase separation and gene control. *Science.* **361**, eaar3958
23. Whyte, W.A., Orlando, D.A., Hnisz, D., Abraham, B.J., Lin, C.Y., Kagey, M.H., Rahl, P.B., Lee, T.I., and Young, R.A. (2013) Master transcription factors and mediator establish super-enhancers at key cell identity genes. *Cell.* **153**, 309-319
24. Hnis, D., Abraham, B., Lee, T.I., Lau, A., Saint-André, V., Sigova, A.A., Hoke, H.A., and Young, R.A. (2013) Super-enhancers in the control of cell identity and disease. *Cell.* **155**, 934-947
25. Tan, M., Pan, Q., Gong, H., Zhai, X., Wan, Z., Ge, M., Gu, J., Zhang, D., Chen, X., and Xu, D. (2023) Super-enhancer-associated SNHG15 cooperating with FOSL1 contributes to bladder cancer progression through the WNT pathway. *Pharmacol. Res.* **197**, 106940
26. Luo, S., Luo, Y., Wang, Z., Yin, H., Wu, Q., Du, X., and Xie, X. (2024) Super-enhancer mediated upregulation of MYEOV suppresses ferroptosis in lung adenocarcinoma. *Cancer Lett.* **589**, 216811
27. Hu, X., Wu, J., Feng, Y., Ma, H., Zhang, E., Zhang, C., Sun, Q., Wang, T., Ge, Y., Zong, D., et al. (2023) METTL3-stabilized super enhancers-lncRNA SUCLG2-AS1 mediates the formation of a long-range chromatin loop between enhancers and promoters of SOX2 in metastasis and

radiosensitivity of nasopharyngeal carcinoma. *Clin. Transl. Med.* **13**, e1361

28. Tasdemir, N., Banito, A., Roe, J.S., Alonso-Curbelo, D., Camiolo, M., Tschaharganeh, D.F., Huang, C.H., Aksoy, O., Bolden, J.E., Chen, C.C., et al. (2016) BRD4 connects enhancer remodeling to senescence immune surveillance. *Cancer Discov.* **6**, 612-629
29. Li, G.H., Qu, Q., Qi, T.T., Teng, X.Q., Zhu, H.H., Wang, J.J., Lu, Q., and Qu, J. (2021) Super-enhancers: a new frontier for epigenetic modifiers in cancer chemoresistance. *J. Exp. Clin. Cancer Res.* **40**, 174
30. Guo, Q., Quan, M., Dong, J., Bai, J., Wang, J., Han, R., Wang, W., Cai, Y., et al. (2020) The WW domains dictate isoform-specific regulation of YAP1 stability and pancreatic cancer cell malignancy. *Theranostics* **10**, 4422-4436
31. Ganser, L.R., and Myong, S. (2020) Methods to Study Phase-Separated Condensates and the Underlying Molecular Interactions. *Trends Biochem Sci.* **45**, 1004-1005
32. Kaneda, A., Seike, T., Danjo, T., Nakajima, T., Otsubo, N., Yamaguchi, D., Tsuji, Y., Hamaguchi, K., Yasunaga, M., Nishiya, Y., et al. (2020) The novel potent TEAD inhibitor, K-975, inhibits YAP1/TAZ-TEAD protein-protein interactions and exerts an anti-tumor effect on malignant pleural mesothelioma. *Am. J. Cancer Res.* **10**, 4399-4415
33. Lu, Y., Wu, T., Gutman, O., Lu, H., Zhou, Q., Henis, Y.I., and Luo, X. (2020) Phase separation of TAZ compartmentalizes the transcription machinery to promote gene expression. *Nat. Cell Biol.* **22**, 453-464
34. Hatstat, A.K., Pupi, M.D., and McCafferty, D.G. (2021) Predicting PY motif-mediated protein-protein interactions in the Nedd4 family of ubiquitin ligases. *PLoS One* **16**, e0258315
35. Mehta, S., and Zhang, J. (2022) Liquid-liquid phase separation drives cellular function and dysfunction in cancer. *Nat. Rev. Cancer* **22**, 239-252
36. Qian, H., Zhu, M., Tan, X., Zhang, Y., Liu, X., and Yang, L. (2023) Super-enhancers and the super-enhancer reader BRD4: tumorigenic factors and therapeutic targets. *Cell Death Discov.* **9**, 470

37. Conaway, R.C., and Conaway, J.W. (2011) Function and regulation of the mediator complex. *Curr. Opin. Genet. Dev.* **21**, 225-230
38. Blumenthal, D., Goldstien, L., Edidin, M., and Gheber, L.A. (2015) Universal Approach to FRAP Analysis of Arbitrary Bleaching Patterns. *Sci Rep* **5**, 11655
39. Han, X., Yu, D., Gu, R., Jia, Y., Wang, Q., Jaganathan, A., Yang, X., Yu, M., Babault, N., Zhao, C., et al. (2020) Roles of the BRD4 short isoform in phase separation and active gene transcription. *Nat. Struct. Mol. Biol.* **27**, 333-341
40. Chung, V.Y., Tan, T.Z., Ye, J., Huang, R.L., Lai, H.C., Kappei, D., Wollmann, H., Guccione, E., and Huang, R.Y. (2019) The role of GRHL2 and epigenetic remodeling in epithelial-mesenchymal plasticity in ovarian cancer cells. *Commun Biol.* **2**, 272
41. Jovanović, B., Temko, D., Stevens, L.E., Seehawer, M., Fassl, A., Murphy, K., Anand, J., Garza, K., Gulvady, A., Qiu, X., et al. (2023) Heterogeneity and transcriptional drivers of triple-negative breast cancer. *Cell Rep.* **42**, 113564
42. Filippakopoulos, P., Qi, J., Picaud, S., Shen, Y., Smith, W.B., Fedorov, O., Morse, E.M., Keates, T., Hickman, T.T., Felletar, I., et al. (2010) Selective inhibition of BET bromodomains. *Nature* **468**, 1067-1073
43. Cerami, E., Gao, J., Dogrusoz, U., Gross, B.E., Sumer, S.O., Aksoy, B.A., Jacobsen, A., Byrne, C.J., Heuer, M.L., Larsson, E., et al. (2012) The cBio cancer genomics portal: an open platform for exploring multidimensional cancer genomics data. *Cancer Discov.* **2**, 401-404
44. Gao, J., Aksoy, B.A., Dogrusoz, U., Dresdner, G., Gross, B., Sumer, S.O., Sun, Y., Jacobsen, A., Sinha, R., Larsson, E., et al. (2013) Integrative analysis of complex cancer genomics and clinical profiles using the cBioPortal. *Sci. Signal.* **6**, pl1
45. de Bruijn, I., Kundra, R., Mastrogiacomo, B., Tran, T.N., Sikina, L., Mazor, T., Li, X., Ochoa, A., Zhao, G., Lai, B., et al. (2023) Analysis and visualization of longitudinal genomic and clinical data from the AACR

project GENIE Biopharma Collaborative in cBioPortal. *Cancer Res*. **83**, 3861-3867

46. Ryan, M., Wong, W.C., Brown, R., Akbani, R., Su, X., Broom, B., Melott, J., and Weinstein, J. (2016) TCGASpliceSeq a compendium of alternative mRNA splicing in cancer. *Nucleic Acids Res*. **44**, D1018-D1122
47. Fenouille, N., Tichet, M., Dufies, M., Pottier, A., Mogha, A., Soo, J.K., Rocchi, S., Mallavialle, A., Galibert, M.D., Khammari, A., et al. (2012) The epithelial-mesenchymal transition (EMT) regulatory factor SLUG (SNAI2) is a downstream target of SPARC and AKT in promoting melanoma cell invasion. *PLoS One*. **7**, e40378
48. McLean, M.E., MacLean, M.R., Cahill, H.F., Arun, R.P., Walker, O.L., Wasson, M.D., Fernando, W., Venkatesh, J., and Marcato, P. (2023) The Expanding Role of Cancer Stem Cell Marker ALDH1A3 in Cancer and Beyond. *Cancers*. **15**, 492
49. Bauzone, M., Souidi, M., Dessein, A.F., Wisztorski, M., Vincent, A., Gimeno, J.P., Monté, D., Van Seuningen, I., Gespach, C., and Huet, G. (2021) Cross-talk between YAP and RAR-RXR Drives Expression of Stemness Genes to Promote 5-FU Resistance and Self-Renewal in Colorectal Cancer Cells. *Mol Cancer Res*. **19**, 612-622
50. Xiao, Y., Zhang, H., Ma, Q., Huang, R., Lu, J., Liang, X., Liu, X., Zhang, Z., Yu, L., Pang, J., Zhou, L., Liu, T., Wu, H., and Liang, Z. (2019) YAP1-mediated pancreatic stellate cell activation inhibits pancreatic cancer cell proliferation. *Cancer Lett*. **462**, 51-60
51. Guo, X., Tai, H., Li, X., Liu, P., Liu, J., and Yu, S. (2024) SPARC is a Novel Prognostic Biomarker for Ovarian Cancer and Associated with Immune Signatures and Drug Response. *Clin. Exp. Obstet. Gynecol*. **51**, 61
52. Chen, J., Wang, M., Xi, B., Xue, J., He, D., Zhang, J., and Zhao, Y. (2012) SPARC is a key regulator of proliferation, apoptosis and invasion in human ovarian cancer. *PLoS One*. **7**, e42413
53. Huang, J., Tang, Y., Li, Y., Wei, W., Kang, F., Tan, S., Lin, L., Lu, X., Wei, H., and Wang, N. (2024) ALDH1A3 contributes to tumorigenesis in high-

grade serous ovarian cancer by epigenetic modification. *Cell Signal*. **116**, 111044

54. Dart, A. (2023) EMT in chemoresistance. *Nat. Rev. Cancer*. **23**, 349
55. Hanahan, D., and Weinberg, R.A. (2000) The hallmarks of cancer. *Cell*. **100**, 57-70
56. Zhang, C., Yang, Z., Dong, D.L., Jang, T.S., Knowles, J.C., Kim, H.W., Jin, G.Z., and Xuan, Y. (2020) 3D culture technologies of cancer stem cells: promising ex vivo tumor models. *J. Tissue Eng.* **11**, 1-17
57. Zhang, C., Liu, X., Jin, S., Chen, Y., and Guo, R. (2022) Ferroptosis in cancer therapy: a novel approach to reversing drug resistance. *Mol Cancer*. **21**, 47
58. Lord, C., and Ashworth, A. (2016) BRCAness revisited. *Nat Rev Cancer* **16**, 110-120
59. Moffitt, R.A., Marayati, R., Flate, E.L., Volmar, K.E., Loeza, S.G., Hoadley, K.A., Rashid, N.U., Williams, L.A., Eaton, S.C., Chung, A.H., et al. (2015) Virtual microdissection identifies distinct tumor- and stroma-specific subtypes of pancreatic ductal adenocarcinoma. *Nat Genet*. **47**, 1168-1178.
60. Monster, J.L., Kemp, L.J.S., Gloerich, M., and van der Post, R.S. (2022) Diffuse gastric cancer: Emerging mechanisms of tumor initiation and progression. *Biochim Biophys Acta Rev Cancer*. **1877**, 188719
61. Kaan, H.Y.K., Chan, S.W., Tan, S.K.J., Guo, F., Lim, C.J., Hong, W., and Song, H. (2017) Crystal structure of TAZ-TEAD complex reveals a distinct interaction mode from that of YAP-TEAD complex. *Sci. Rep*. **7**, 2035
62. Cunningham, R., and Hansen, C.G. (2022) The Hippo pathway in cancer: YAP/TAZ and TEAD as therapeutic targets in cancer. *Clin. Sci.* **136**, 197-222
63. Yu, M., Peng, Z., Qin, M., Liu, Y., Wang, J., Zhang, C., Lin, J., Dong, T., Wang, L., Li, S., et al. (2021) Interferon-γ induces tumor resistance to anti-PD-1 immunotherapy by promoting YAP phase separation. *Mol. Cell* **81**, 1216-1230

64. Cai, D., Feliciano, D., Dong, P., Flores, E., Gruebele, M., Porat-Shliom, N., Sukenik, S., Liu, Z., and Lippincott-Schwartz, J. (2019) Phase separation of YAP reorganizes genome topology for long-term YAP target gene expression. *Nat Cell Biol*. **21**, 1578-1589
65. Bangru, S., Arif, W., Seimetz, J., Bhate, A., Chen, J., Rashan, E.H., Carstens, R.P., Anakk, S., and Kalsotra, A. (2018) Alternative splicing rewires Hippo signaling pathway in hepatocytes to promote liver regeneration. *Nat Struct Mol Biol*. **25**, 928-939.
66. Wang, G., Lu, X., Dey, P., Deng, P., Wu, C.C., Jiang, S., Fang, Z., Zhao, K., Konaparthi, R., Hua, S., et al. (2016) Targeting YAP-dependent MDSC infiltration impairs tumor progression. *Cancer Discov*. **6**, 80-95
67. Yang, W., Yang, S., Zhang, F., Cheng, F., Wang, X., and Rao, J. (2020) Influence of the Hippo-YAP signalling pathway on tumor associated macrophages (TAMs) and its implications on cancer immunosuppressive microenvironment. *Ann. Transl. Med*. **8**, 399
68. Ooki, T., Murata-Kamiya, N., Takahashi-Kanemitsu, A., Wu, W., and Hatakeyama, M. (2019) High-Molecular-Weight hyaluronan is a Hippo pathway ligand directing cell density-dependent growth inhibition via PAR1b. *Dev. Cell* **49**, 590-604
69. Ge, S.X., Son, E.W., and Yao, R. (2018) iDEP: an integrated web application for differential expression and pathway analysis of RNA-Seq data. *BMC Bioinformatics*. **19**, 534
70. Ge, S.X., Jung, D., and Yao, R. (2020) ShinyGO: a graphical gene-set enrichment tool for animals and plants. *Bioinformatics*. **36**, 2628-2629
71. Rauluseviciute, I., Riudavets-Puig, R., Blanc-Mathieu, R., Castro-Mondragon, J.A., Ferenc, K., Kumar, V., Lemma, R.B., Lucas, J., Chèneby, J., Baranasic, D., et al. (2024) JASPAR 2024: 20th anniversary of the open-access database of transcription factor binding profiles. *Nucleic Acids Res*. **52**, D174-D182

Figure Legends

Figure 1. YAP1 induces LLPS in a splicing isoform dependent manner. *A*, Schematic diagram of YAP1 isoforms. *B-D*, *YAP1*-KO UWB1.289 cells were transfected with YAP1 isoforms fused to mVenus at the C-terminus. Immunoblotting of endogenous YAP1-1 (indicated by *), YAP1-2 (indicated by **) in parental UWB1.289 cells, and of mVenus-YAP1 isoforms in *YAP1*-KO UWB1.289 cells (*B*). Number of mVenus-YAP1 puncta per nucleus. ***$p < 0.001$ (Mann-Whitney U test). n=88 (average) nuclei per group (range; 83-93 nuclei) (*C*). See Fig. S1*B* for the cell populations used in the analysis. The fluorescence signal of mVenus (green) and DAPI (blue) (*D*). *E-F*, Reconstitution of *YAP1*-KO UWB1.289 cells with a single YAP1 isoform, YAP1-2α or YAP1-2γ. Established clone cells were subjected to an immunoblotting analysis using indicated antibodies (*E*) and immunofluorescence staining using a YAP1 antibody (*F*). *G-H*, Live cell imaging of *YAP1*-KO UWB1.289 cells transfected with mVenus-YAP1-2α. YAP1-2α fluorescence signals at the indicated time points after Hex treatment (*G*). Fusion event of YAP1-2α puncta. Yellow arrows indicate punctate fusion (*H*). *I-J*, FRAP analysis of mVenus-YAP1-2α. Time-lapse images of two different *YAP1*-KO UWB1.289 cells transfected with mVenus-YAP1-2α are shown in Exp.1 and Exp.2. Yellow arrows indicate photobleached puncta. Images of the entire nucleus are shown in Figure S1*G*. Unbleached puncta were used as negative controls. Scale bars indicate 1 μm (*I*). Fluorescence intensities of puncta

(photobleached, n=12; unbleached, n=12) were analyzed from a series of time-lapse images. *D*: diffusion coefficient. Error bars indicate the mean ± SD (*J*). (*D*, *F*-*H*) Scale bars indicate 10 μm.

Figure 2. YAP1-2α/TAZ/TEAD enhancer complex initiated by YAP1-2α/TAZ heterodimerization is required for YAP1 LLPS. *A*, Fluorescence images of mVenus-fused YAP1-2α (green) and mCherry-fused TAZ (red) (top panels). The colocalization of YAP1-2α and TAZ in the puncta was shown as white signals (bottom). *B*, Nuclear puncta formation in *YAP1*-KO UWB1.289 cells expressing the mVenus-fused YAP1-2α mutants (left). Number of YAP1 puncta in the nucleus (right). n=75 cells in each group. *C*, Formation of YAP1-2α puncta in the *TAZ*-KO UWB1.289 cells or knockout control UWB1.289 cells (left). Number of YAP1 puncta in the nucleus (right). n=100 cells in each group. *D*-*E*, Artificial heterodimerization between YAP1-2α(LZM) and TAZ(LZM), or YAP1-2γ and TAZ(LZM) in UWB1.289 cells using the iDimerize Induceble Heterodimer System (Clontech). Schematic view (*D*). Number of YAP1 puncta in the nucleus. n=50 (left) or 40 (right) cells in each group. DmrA-mVenus is used as control (*E*). Confirmation of heterodimer formation and immunofluorescence images were shown in Figure S2, *K*-*L*. *F*, Immunofluorescence images of mVenus-fused YAP1-2α (green) and pan-TEAD (red). The puncta indicated by white arrows are enlarged. *G*, Wild-type YAP1-2α(WT) or YAP1-2α(S94A)-transfected UWB1.289 cells were

treated with K-975. Immunofluorescence images of YAP1-2α (left). Number of YAP1 puncta in the nucleus (right). n=60 cells in each group. *H*, UWB1.289 cells were co-transfected with mSECFP-fused YAP1-2α, mVenus-fused HA-TAZ, and Flag-TAZ and analyzed by combining FRET and PLA to detect YAP1-2α/TAZ heterodimers and TAZ/TAZ homodimers in YAP1-2α or TAZ/TAZ puncta. TAZ homodimer was visualized using PLA (red). YAP1-2α/TAZ heterodimer was detected by SECFP/Venus FRET. White arrows indicate YAP1-2α/TAZ-LLPS puncta, yellow arrows indicate TAZ/TAZ-LLPS puncta. Low magnification images (left) and enlarged images the area outlined in yellow dotted lines in left panels (right). (*B*-*C*, *E*, *G*) ***$p < 0.001$; n.s., not significant (Mann-Whitney U test). Red lines represent the mean value. All scale bars represent 10 μm.

Figure 3. Multivalent association between YAP1-2α/TAZ/TEAD complex and BRD4 via the YAP1 WW domain is essential for YAP1 LLPS. *A*, Schematic diagram of BRD4. BRD4 has two WW domain-binding motifs. PPxY or LPxY: WW domain-binding motifs. *B*-*C*, Interaction between HA-YAP1-2α and Flag-BRD4 mutants in UWB1.289 and MDA-MB-436 cells were examined by PLA or anti-Flag immunoblotting analysis of anti-HA immunoprecipitates. HA-YAP1-2α expressing MDA-MB-436 cells were transfected with indicated Flag-BRD4 mutant and subjected to an IP experiment. Total cell lysates (TCL) were put as input samples (*B*; left). The relative interaction between YAP1-

2α and BRD4 was calculated by defining Flag-BRD4 (WT) intensity per HA-YAP1-2α intensity in the IP sample as one. n=3, biological replicates. Error bars indicate the mean ± SD (*B*; right). PLA was performed in UWB1.289 cells infected with the lentivirus transducing HA-YAP1-2α and indicated BRD4 mutants. PL spots indicate interaction between HA-YAP1-2α and Flag-BRD4 (*C*; left). Number of nuclear PL spots was shown in graph. n=40 nuclei for each group (*C*; right). *D*-*E*, Effect of BRD4 inhibition on mCherry-fused YAP1-2α puncta formation in UWB1.289 cells (*D*; left) and MDA-MB-436 cells (*D*; right). BRD4 was knocked down using two different shRNAs (#1 and #2). Cells transfected with shBRD4 were marked by GFP (green). mCherry-fused YAP1-2α (red). The number of YAP1-2α puncta in the nucleus was calculated. n=60 (left) or 50 (right) nuclei for each group (*E*; top). BRD4 knockdown was confirmed by immunoblotting (*E*; bottom). *F*, Genetic rescue of the shBRD4-mediated reduction in YAP1-2α puncta formation by indicated shBRD4-resistant BRD4 mutant (left; UWB1.289, right; MDA-MB-436). n=20 nuclei for each group. *G*-*H*, Loss-of-function WW domain mutants were created by introducing point mutations into WW domains of YAP1-2α ($WW1^{mut}$: W199A+P202A, $WW2^{mut}$: W258A+P261A, $WW1/2^{mut}$: W199A+P202A|W258A+P261A). The binding ability between YAP1-WW domain mutants and BRD4 was evaluated using PLA. n=300 nuclei for each group (*G*). The effect of loss-of-function of WW domain in UWB1.289 cells on nuclear YAP1 puncta formation was evaluated by

immunofluorescence staining. n=300 nuclei for each group (*H*). ***p < 0.001; **p < 0.01; *p < 0.05; n.s., not significant (*B*: Student's T test; *C*, *E-H*: Mann-Whitney U test). Red bars indicate the mean value (*C*, *E-H*). All scale bars represent 10 μm.

Figure 4. YAP1-2α/TAZ/TEAD/BRD4 complex accumulates at super-enhancer elements. *A-D*, The expression level of typical TEAD target gene (*CCN1*) was analyzed by qPCR. UWB1.289 cells transduced with the indicated YAP1 isoforms using lentiviruses (*A*). HA-YAP1-2α or empty vector transfected *TAZ*-KO or KO control UWB1.289 cells (*B*). HA-YAP1-2α(WT), HA-YAP1-2α(LZM) or empty vector transfected UWB1.289 cells (*C*). Artificial heterodimerization between YAP1-2α(LZM) and TAZ(LZM), or YAP1-2γ and TAZ(LZM) in UWB1.289 cells using the iDimerize Induceble Heterodimer System, shown as Figure 2*E* (*D*). *E*, Prediction of potential TEAD-positive super-enhancer elements upstream of the *CCN1* gene. The identified super-enhancer elements in serous ovarian cancer cells (GSM3328052: PEO1 cells) and triple-negative breast cancer cells (GSM6132824: MDA-MB-436 cells) are shown in first and second line from the top. The TEAD-binding motif sequences were predicted using JASPR. Potential TEAD-positive super-enhancer elements upstream of *CCN1* gene were indicated as red lines (-0.3 kb or -0.85 kb from TSS). *F*, In UWB1.289 cells where endogenous YAP1 was replaced with HA-YAP1-2α or HA-YAP1-2γ (see Figure 1*E-F*), the enrichment levels of super-

enhancer marker BRD4, HA-tagged YAP1, TAZ, and TEAD at predicted super-enhancer elements were evaluated by qPCR. The DNA templates were prepared using CUT & RUN with the indicated antibodies. *G-H*, Analysis of YAP1-2α/TAZ/TEAD complex binding to the predicted super-enhancer regions in 6xHis-YAP1-2α expressing *YAP1*-KO UWB1.289 cells. The DNA or protein samples were prepared using ChIP-re-chip. Formation of YAP1-2α/TAZ/TEAD complex in the cells treated with K975 or DMSO was confirmed by immunoblotting following ChIP-re-chip (*G*). Enrichment of YAP1-2α/TAZ/TEAD complex on predicted super-enhancer regions was evaluated by ChIP-re-chip-qPCR analysis (*H*). *I*, The effect of JQ1 treatment on the increase in *CCN1* expression mediated by YAP1-2α was analyzed using qPCR. (*A-D*, *F*, *H-I*) ***p < 0.001; **p < 0.01, *p < 0.05, (*A-C*, *F*, *H-I*: Welch's T test, *D*: Student's T test). n=3 (technical replicates). Plots indicate RQ (relative quantification) for each sample. Error bars indicate the mean ± SD.

Figure 5. Highly expressed YAP1-2α correlates with EMT signature in HGSOC patients. *A-B*, HGSOC patients (n = 425) were divided into the "*YAP1-*$\alpha^{dominant}$" (n = 131), "*YAP1-*$\beta^{dominant}$" (n = 83), "*YAP1-*$\gamma^{dominant}$" (n = 78), and "*YAP1-*$\delta^{dominant}$" (n = 133). Genes whose expression increased in "*YAP1-*$\alpha^{dominant}$" vs. "*YAP1-*$\gamma^{dominant}$" (FDR < 0.1, FC >1.5) or deceased in "*YAP1-*$\alpha^{dominant}$" vs. "*YAP1-*$\gamma^{dominant}$" (FDR < 0.1, FC <1.5) were shown in volcano plot (*A*). Gene-set enrichment analysis of increased genes

(Hallmark MSigDB). The size of circle indicates number of enrichment genes. The -log10(FDR) value is represented in blue (high) to red (low)(*B*). *C*, The expression level of EMT/stemness related genes were analyzed by qPCR. UWB1.289 cells transduced with the indicated YAP1 isoforms using lentiviruses were treated with JQ1 or DMSO as a mock control. *SPARC* (left), *ALDH1A3* (center), and *SNAI2* (right). *D*, The effect of JQ1 treatment on the formation of YAP1-2α-LLPS puncta was analyzed using immunofluorescence staining. Green: HA-tagged YAP1 (left). Number of YAP1 puncta in the nucleus. Plots indicate average of nuclear YAP1 puncta in each experiment (n > 100 nuclei, three biological replicate experiments) (right). Scale bars represent 10 μm. *E*, In UWB1.289 cells where endogenous YAP1 was replaced with HA-YAP1-2α or HA-YAP1-2γ (see Figure 1*C*), the enrichment levels of super-enhancer marker BRD4, YAP1 (HA-tag), TAZ, and TEAD at potential super-enhancer elements (left: *SPARC*; -0.67 kb from TSS, right: *SPARC*; -3.2 kb from TSS) were evaluated by qPCR. The DNA templates were prepared using CUT & RUN with the indicated antibodies. *F*, *TAZ*-KO or KO control UWB1.289 cells were transfected with HA-YAP1-2α or an empty vector as control. The mRNA expression levels of *SPARC* (left) and *ALDH1A3* (right) were assessed by qPCR. Relative mRNA expression levels were calculated with cells transfected with an empty vector as one. (*C*-*F*) ***p < 0.001; **p < 0.01, *p < 0.05, n.s., not significant (Welch's T test). Error bars indicate the mean ± SD. (*C*, *E*-*F*) n=3 (technical replicates). Plots indicate RQ for each sample.

Figure 6. YAP1-2α strengthens cancer cell robustness and potentiates malignant characteristics. *A*, YAP1-2α-overexpressing or control UWB1.289 spheroids were treated with K-975, JQ1, or DMSO as a mock-treated control. Bright-field images and ki-67 staining of 3D-cultured spheroids. Scale bars represent 100 μm. The Feret diameter of the spheroids is shown in the graph (bottom right). Red bars represent mean values. ***$p < 0.001$; **$p < 0.01$ (Student's T test), $n > 230$ spheroids in each group. *B-E*, YAP1-2α-overexpressing or YAP1-2γ-overexpressing UWB1.289 cells were treated with K-975, JQ1 or DMSO as a mock-treated control, followed by chemotaxis (*B*), matrix invasion (*C*), ferroptosis assay (*D*), Cisplatin sensitivity assay (*E*). Chemotaxis capacity or matrix invasion ability was analyzed using transwell. The number of cells that migrated or invaded into the lower well was measured by detecting ATP content (*B-C*). Chlorido [N, N'-Disalicylidene-1,2-Phenylenediamine] Iron (III) was used as ferroptosis inducer. Cell viability was measured by detecting ATP content. Relative cell viability was calculated as the ratio of cells treated with ferroptosis inducer to untreated cells within each group (*D*). Sensitivity to Cisplatin was measured using an MTS assay (*E*). (*B-E*) n=3 (technical replicates). ***$p < 0.001$; n.s., not significant (Welch's T test). Error bars indicate mean ± SD. *F-K*, Artificial heterodimerization between YAP1-2α(S127A-LZM)-WW1/2^{WT}, or YAP1-2α(S127A-LZM)-WW1/2^{mut} and TAZ(LZM) in UWB1.289 cells using the

iDimerize Inducible Heterodimer System. Immunofluorescence images (*F*). Confirmation of heterodimer formation and BRD4 interaction were shown in Figure S6*D*. Anchorage-independent growth (*G*), chemotaxis (*H*), matrix invasion (*I*), ferroptosis assay (*J*), Cisplatin sensitivity assay (*K*). (*G-K*) n=3 (technical replicates). ***p < 0.001; **p < 0.01; **p < 0.05; n.s., not significant (*G-H*, *J*: Welch's T test, *I*: Student's T test). Error bars indicate mean ± SD. *L-P*, Analysis of sequential tissue sections derived from patients with high-grade serous ovarian cancer. *YAP1-2α* mRNA or YAP1 protein was visualized using BaseScope or YAP1 immunofluorescence staining and those intensities were quantified using ImageJ software. BaseScope signals (*YAP1-2α* mRNA) (*L*, left panels), HE staining (*L*, right panel), and YAP1 immunofluorescence staining (*M*) in HGSOC patient with high *YAP1-2α* expression (*YAP1-2α* staining score: 3+). Nuclei were stained with DAPI. The dashed box area was enlarged. Scale bars represent 100 μm. The correlation between YAP1 puncta formation (number of YAP1 puncta per cell) and *YAP1-2α* mRNA expression levels (BaseScope intensity per cell) (*N*), clinical stage and YAP1 puncta formation (*O*), or clinical stage and YAP1 intensity per cell (*P*), were shown in graph. ***p < 0.001; **p < 0.01; *p < 0.05; n.s., not significant (Student's T test).

Figure 7. YAP1 splicing switch accelerates the acquisition of Cisplatin resistance. *A*, Inclusion/exclusion of exon 6 in *YAP1* mRNA was determined by agarose gel electrophoresis following PCR using the

primers shown in schematic diagram. Ten independent Cisplatin-resistant UWB1.289 clone cells (R1 to R10) and parental UWB1.289 cells were used. *B*-*C*, UWB1.289 cells transduced with the shRNA targeting *YAP1* or non-targeting shRNA using lentiviruses were subsequently infected with indicated RNAi-resistant HA-YAP1 isoforms. The expression levels of YAP1 were confirmed by immunoblotting (*B*). Sensitivity to Cisplatin was examined using an MTS assay (C). *D*-*E*, Immunofluorescence analysis using anti-YAP1 and anti-TAZ antibodies in parental UWB1.289 and indicated Cisplatin-resistant UWB1.289 clone cells. Immunofluorescence images of YAP1 (green), TAZ (red), and DAPI (blue) (*D*). The fluorescence intensity of YAP1 (green) and TAZ (red) in TAZ puncta (*E*). *F*, Formation of the endogenous YAP1-2α/TAZ/TEAD/BRD4 complex in Cisplatin-resistant clone cells (R2) was examined by immunoblotting analysis of anti-YAP1 immunoprecipitates (left). The relative interactions were calculated by defining the intensity of BRD4, TAZ, or TEAD per intensity of YAP1 in IP sample prepared from parental cells as one (right). $^{**}p < 0.01$; $^{*}p < 0.05$ (Welch's T test). n=3, biological triplicate. *G*-*I*, *TAZ*-KO Cisplatin-resistant UWB1.289 clone cells (R2) transduced with the HA-TAZ using lentiviruses. *TAZ*-KO and HA-TAZ expression were confirmed by immunoblotting (*G*). Effect of *TAZ*-knockout on endogenous YAP1 puncta formation in R2 cells. Immunofluorescence images were shown in Fig. S7*D*. Number of nuclear YAP1 puncta in Parental and R2 cells (*H*). n=60 nuclei for each group. $^{***}p < 0.001$ (Mann-Whitney U test). Red lines indicate the mean value. Sensitivity of indicated cells to

Cisplatin was measured by an MTS assay (*I*). *J*, The effect of TAZ over expression on sensitivity to Cisplatin in parental UWB1.289 cells was analyzed using an MTS assay. (*C*, *I*-*J*) n=3 (technical replicates). Error bars indicate mean ± SD.

Figure 1.

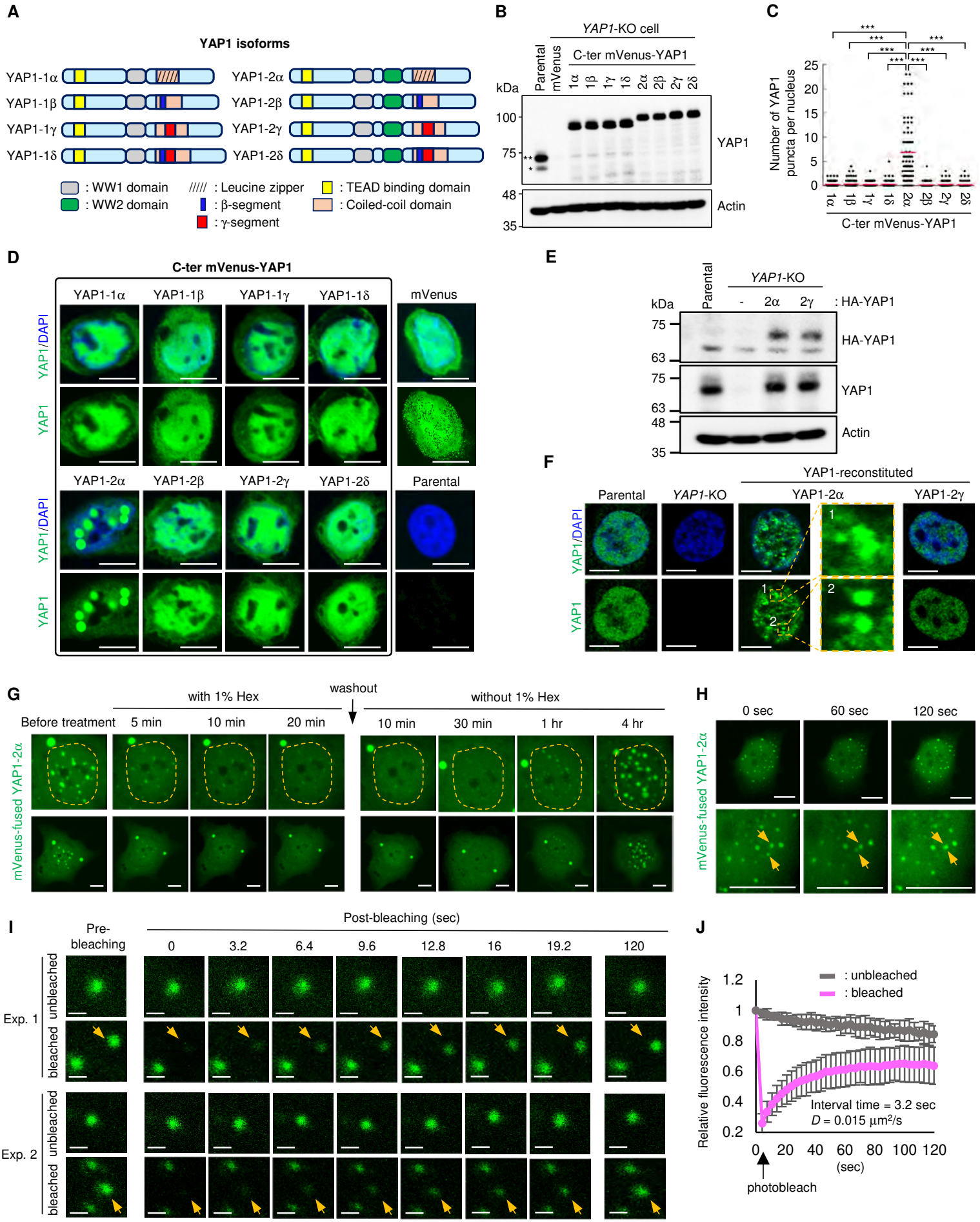
A
YAP1 isoforms
YAP1-1α
YAP1-1β
YAP1-1γ
YAP1-1δ
YAP1-2α
YAP1-2β
YAP1-2γ
YAP1-2δ
: WW1 domain
: WW2 domain
: Leucine zipper
: β-segment
: γ-segment
: TEAD binding domain
: Coiled-coil domain
B
YAP1-KO cell
C-ter mVenus-YAP1
Parental
mVenus
1α 1β 1γ 1δ 2α 2β 2γ 2δ
kDa
100
75
48
35
YAP1
Actin
C
Number of YAP1 puncta per nucleus
C-ter mVenus-YAP1
D
C-ter mVenus-YAP1
YAP1-1α
YAP1-1β
YAP1-1γ
YAP1-1δ
mVenus
YAP1-2α
YAP1-2β
YAP1-2γ
YAP1-2δ
Parental
YAP1/DAPI
YAP1
E
Parental
YAP1-KO
: HA-YAP1
HA-YAP1
YAP1
Actin
F
YAP1-reconstituted
Parental
YAP1-KO
YAP1-2α
YAP1-2γ
YAP1/DAPI
YAP1
G
with 1% Hex
washout
without 1% Hex
Before treatment
5 min
10 min
20 min
10 min
30 min
1 hr
4 hr
mVenus-fused YAP1-2α
H
0 sec
60 sec
120 sec
mVenus-fused YAP1-2α
I
Pre-bleaching
Post-bleaching (sec)
0
3.2
6.4
9.6
12.8
16
19.2
120
Exp. 1
Exp. 2
unbleached
bleached
J
: unbleached
: bleached
Relative fluorescence intensity
Interval time = 3.2 sec
D = 0.015 μm²/s
(sec)
photobleach

Figure 2.

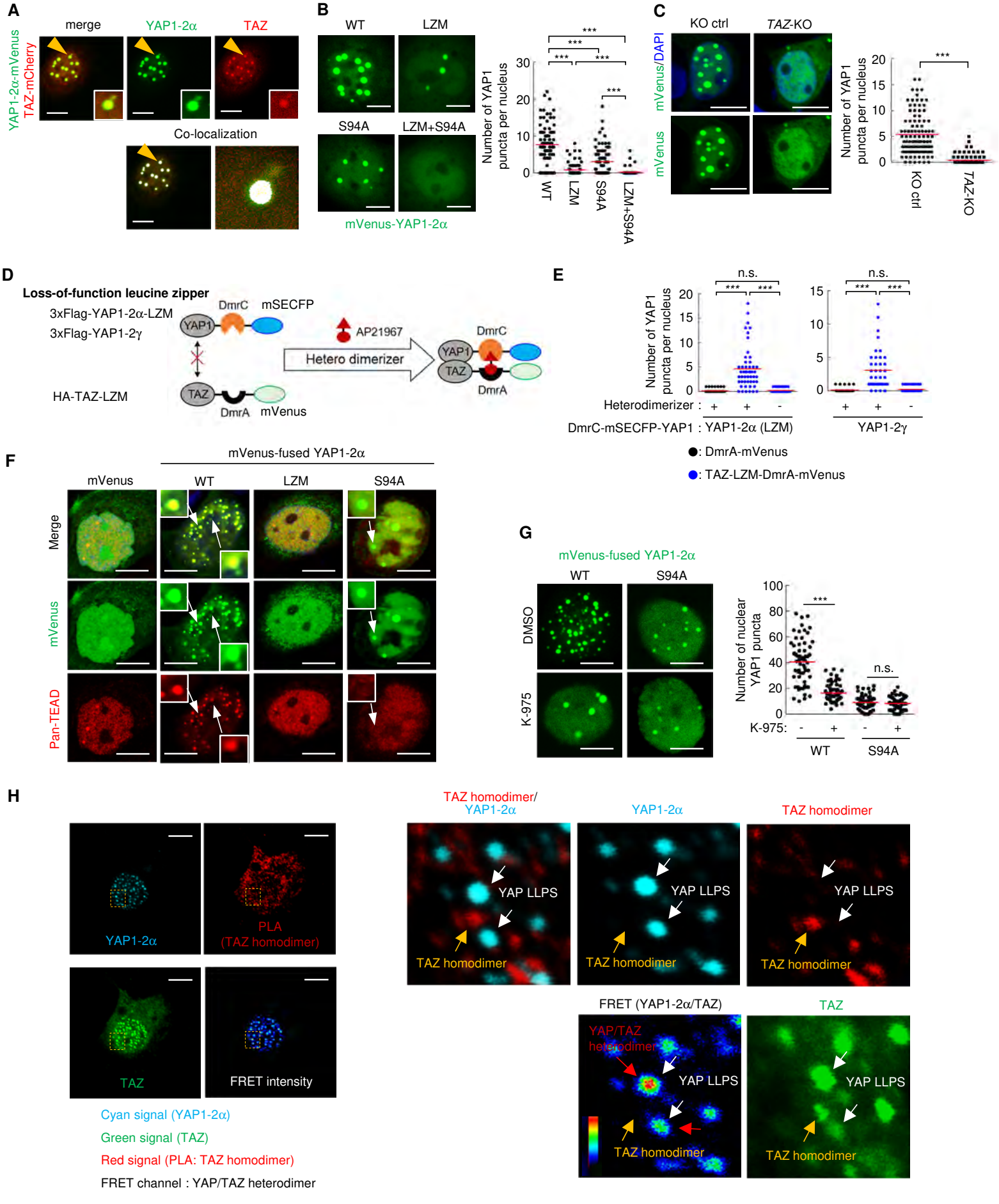
A
merge
YAP1-2α
TAZ
YAP1-2α-mVenus
TAZ-mCherry
Co-localization
B
WT
LZM
S94A
LZM+S94A
mVenus-YAP1-2α
Number of YAP1 puncta per nucleus
C
KO ctrl
TAZ-KO
mVenus/DAPI
mVenus
D
Loss-of-function leucine zipper
3xFlag-YAP1-2α-LZM
3xFlag-YAP1-2γ
HA-TAZ-LZM
DmrC
mSECFP
YAP1
TAZ
DmrA
mVenus
AP21967
Hetero dimerizer
E
n.s.
Heterodimerizer :
DmrC-mSECFP-YAP1 : YAP1-2α (LZM)
YAP1-2γ
●: DmrA-mVenus
●: TAZ-LZM-DmrA-mVenus
F
mVenus-fused YAP1-2α
mVenus
Merge
Pan-TEAD
G
mVenus-fused YAP1-2α
DMSO
K-975
Number of nuclear YAP1 puncta
H
YAP1-2α
PLA (TAZ homodimer)
TAZ
FRET intensity
Cyan signal (YAP1-2α)
Green signal (TAZ)
Red signal (PLA: TAZ homodimer)
FRET channel : YAP/TAZ heterodimer
TAZ homodimer/ YAP1-2α
YAP1-2α
TAZ homodimer
YAP LLPS
FRET (YAP1-2α/TAZ)
YAP/TAZ heterodimer

Figure 3.

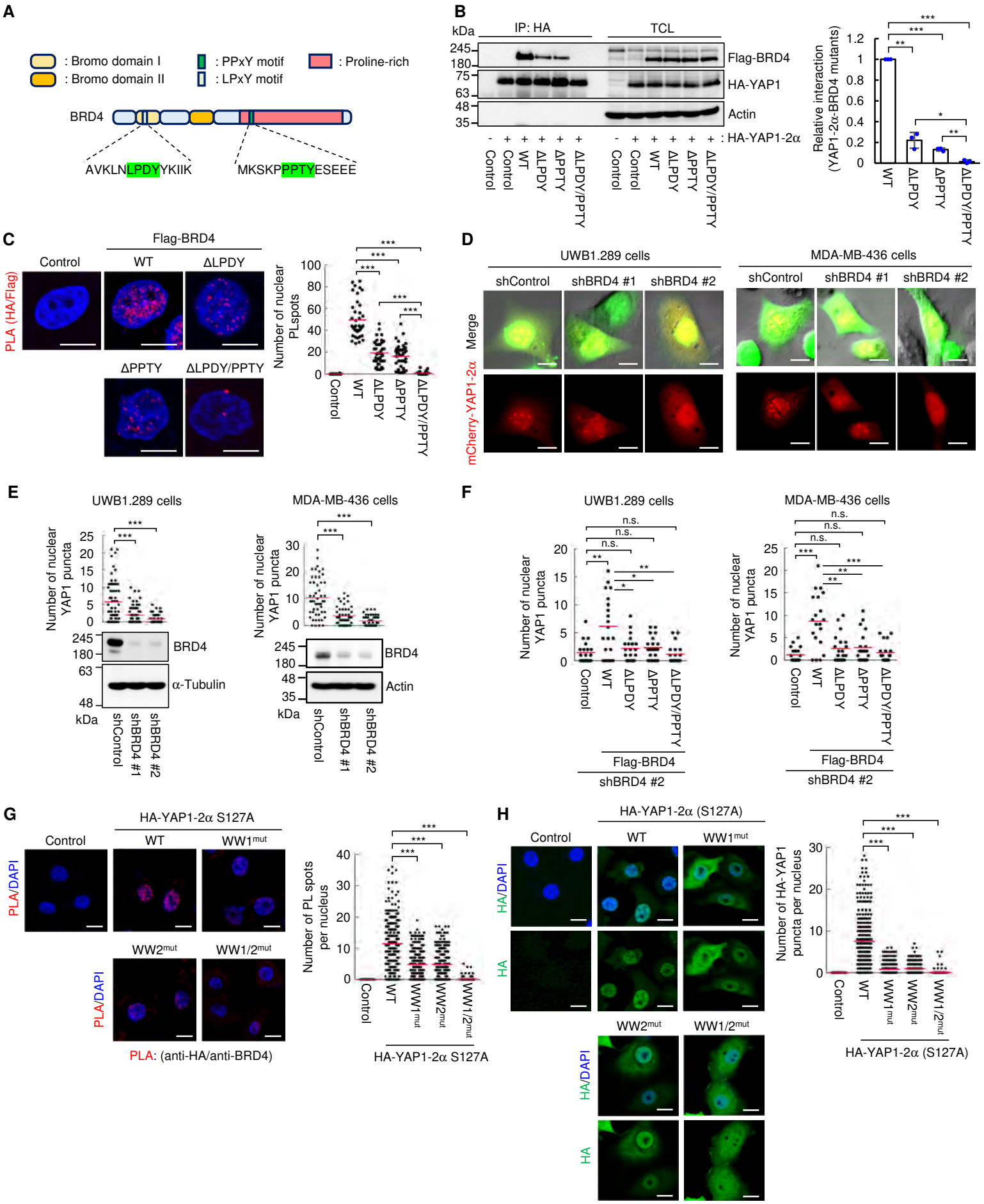
A
: Bromo domain I
: Bromo domain II
: PPxY motif
: LPxY motif
: Proline-rich
BRD4
AVKLNLPDYYKIIK
MKSKPPPTYESEEE
B
kDa
IP: HA
TCL
245
180
75
63
48
35
Flag-BRD4
HA-YAP1
Actin
: HA-YAP1-2α
Control
Control
WT
ΔLPDY
ΔPPTY
ΔLPDY/PPTY
Relative interaction (YAP1-2α-BRD4 mutants)
C
Flag-BRD4
Control
WT
ΔLPDY
ΔPPTY
ΔLPDY/PPTY
PLA (HA/Flag)
Number of nuclear PLspots
D
UWB1.289 cells
MDA-MB-436 cells
shControl
shBRD4 #1
shBRD4 #2
Merge
mCherry-YAP1-2α
E
UWB1.289 cells
MDA-MB-436 cells
Number of nuclear YAP1 puncta
BRD4
α-Tubulin
Actin
kDa
shControl
shBRD4 #1
shBRD4 #2
F
UWB1.289 cells
MDA-MB-436 cells
Number of nuclear YAP1 puncta
n.s.
Control
WT
ΔLPDY
ΔPPTY
ΔLPDY/PPTY
Flag-BRD4
shBRD4 #2
G
HA-YAP1-2α S127A
Control
WT
WW1mut
WW2mut
WW1/2mut
PLA/DAPI
Number of PL spots per nucleus
PLA: (anti-HA/anti-BRD4)
HA-YAP1-2α S127A
H
HA-YAP1-2α (S127A)
Control
WT
WW1mut
WW2mut
WW1/2mut
HA/DAPI
HA
Number of HA-YAP1 puncta per nucleus
HA-YAP1-2α (S127A)

Figure 4.

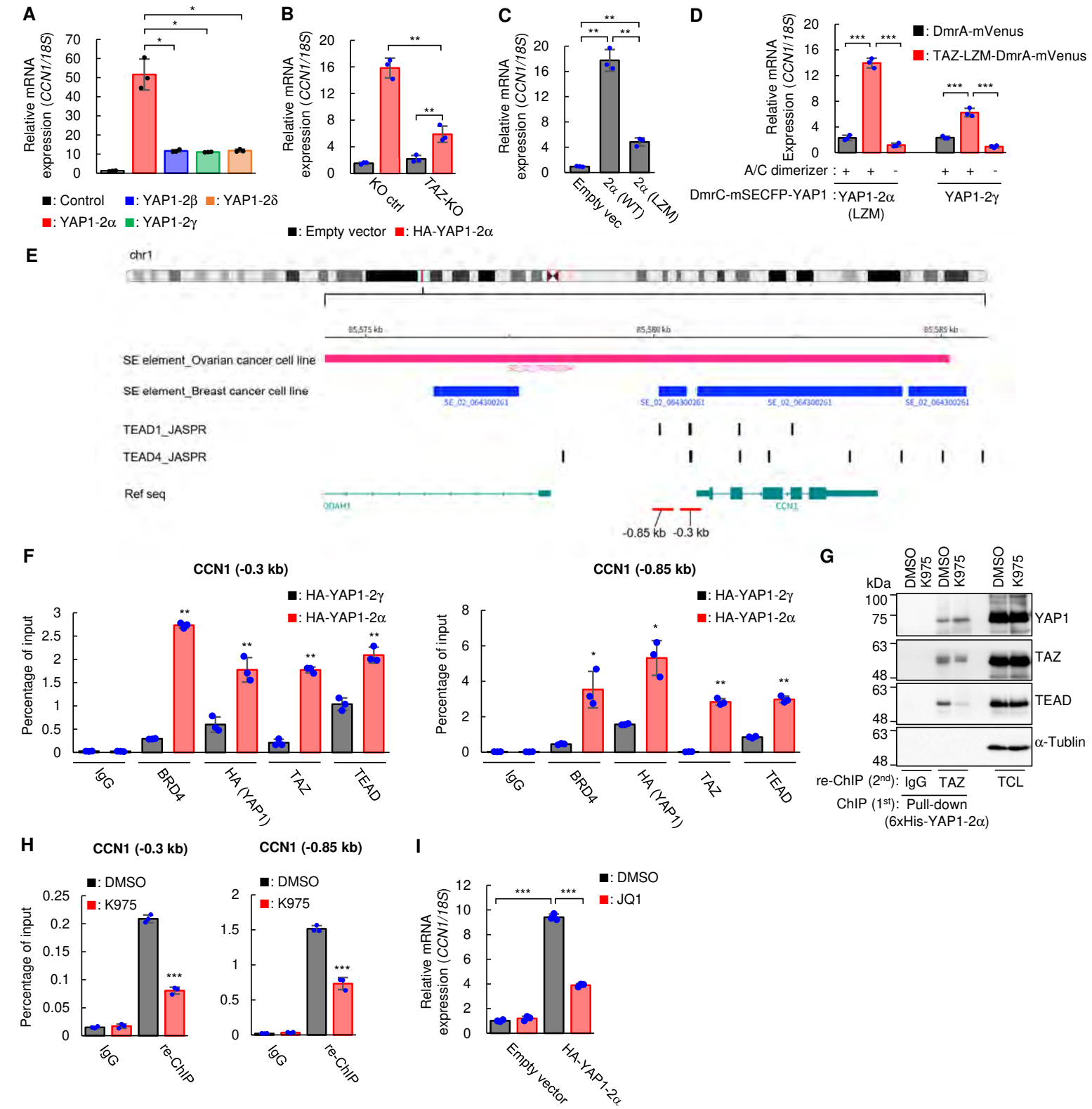
A
Relative mRNA expression (CCN1/18S)
■: Control ■: YAP1-2β ■: YAP1-2δ
■: YAP1-2α ■: YAP1-2γ
B
Relative mRNA expression (CCN1/18S)
KO ctrl
TAZ-KO
■: Empty vector ■: HA-YAP1-2α
C
Relative mRNA expression (CCN1/18S)
Empty vec
2α (WT)
2α (LZM)
D
Relative mRNA Expression (CCN1/18S)
■: DmrA-mVenus
■: TAZ-LZM-DmrA-mVenus
A/C dimerizer : + + - + + -
DmrC-mSECFP-YAP1 : YAP1-2α (LZM) YAP1-2γ
E
chr1
SE element_Ovarian cancer cell line
SE element_Breast cancer cell line
TEAD1_JASPR
TEAD4_JASPR
Ref seq
-0.85 kb -0.3 kb
F
CCN1 (-0.3 kb)
CCN1 (-0.85 kb)
■: HA-YAP1-2γ
■: HA-YAP1-2α
Percentage of input
IgG
BRD4
HA (YAP1)
TAZ
TEAD
G
kDa
DMSO K975 DMSO K975 DMSO K975
YAP1
TAZ
TEAD
α-Tublin
re-ChIP (2nd): IgG TAZ TCL
ChIP (1st): Pull-down (6xHis-YAP1-2α)
H
CCN1 (-0.3 kb)
CCN1 (-0.85 kb)
■: DMSO
■: K975
Percentage of input
IgG
re-ChIP
I
Relative mRNA expression (CCN1/18S)
■: DMSO
■: JQ1
Empty vector
HA-YAP1-2α

Figure 5.

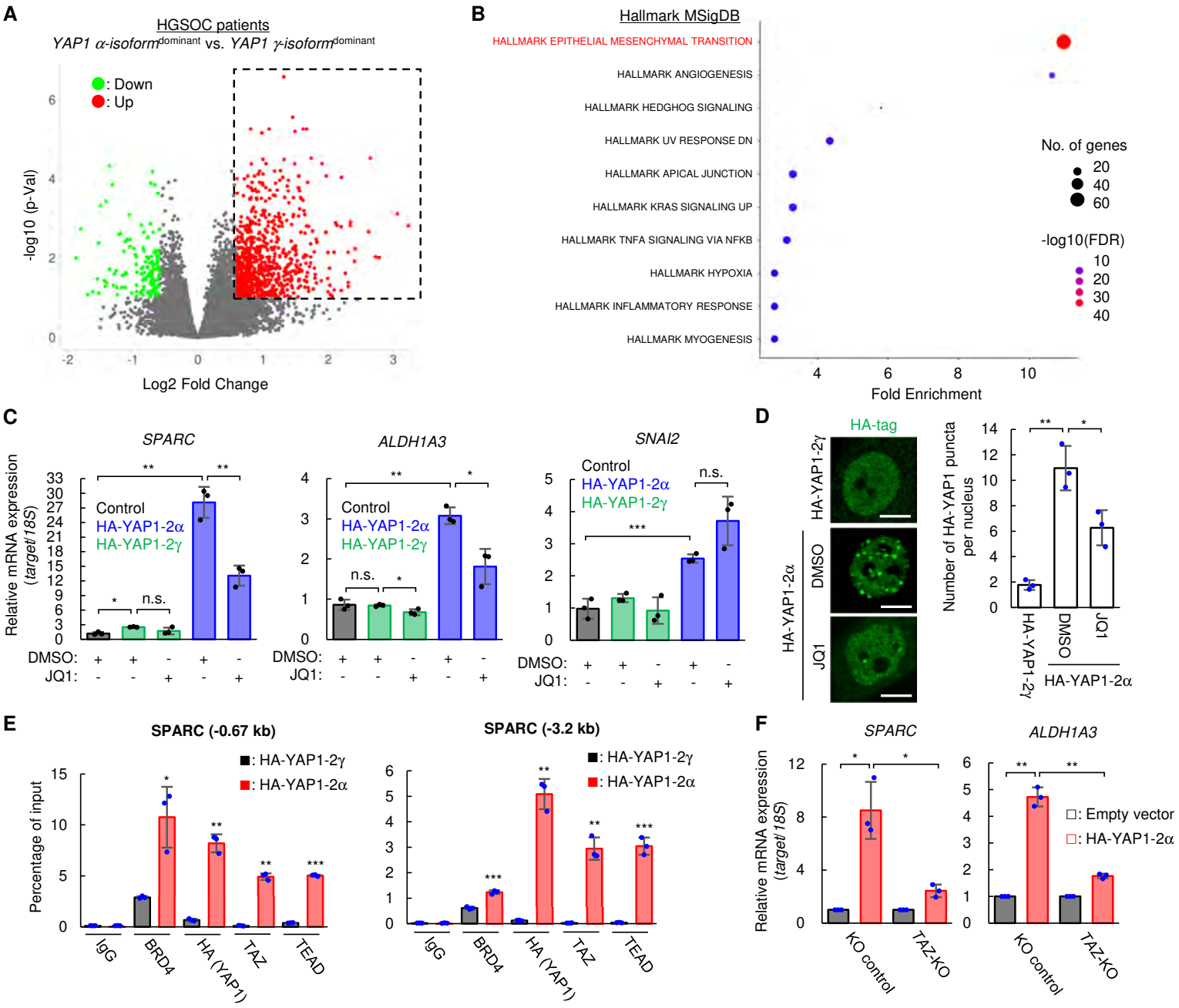
A
HGSOC patients
YAP1 α-isoform dominant vs. YAP1 γ-isoform dominant
: Down
: Up
-log10 (p-Val)
Log2 Fold Change
B
Hallmark MSigDB
HALLMARK EPITHELIAL MESENCHYMAL TRANSITION
HALLMARK ANGIOGENESIS
HALLMARK HEDGHOG SIGNALING
HALLMARK UV RESPONSE DN
HALLMARK APICAL JUNCTION
HALLMARK KRAS SIGNALING UP
HALLMARK TNFA SIGNALING VIA NFKB
HALLMARK HYPOXIA
HALLMARK INFLAMMATORY RESPONSE
HALLMARK MYOGENESIS
Fold Enrichment
No. of genes
-log10(FDR)
C
SPARC
ALDH1A3
SNAI2
Relative mRNA expression (target/18S)
Control
HA-YAP1-2α
HA-YAP1-2γ
n.s.
DMSO:
JQ1:
D
HA-tag
HA-YAP1-2γ
HA-YAP1-2α
DMSO
JQ1
Number of HA-YAP1 puncta per nucleus
E
SPARC (-0.67 kb)
SPARC (-3.2 kb)
: HA-YAP1-2γ
: HA-YAP1-2α
Percentage of input
IgG
BRD4
HA (YAP1)
TAZ
TEAD
F
SPARC
ALDH1A3
Relative mRNA expression (target/18S)
: Empty vector
: HA-YAP1-2α
KO control
TAZ-KO

Figure 6.

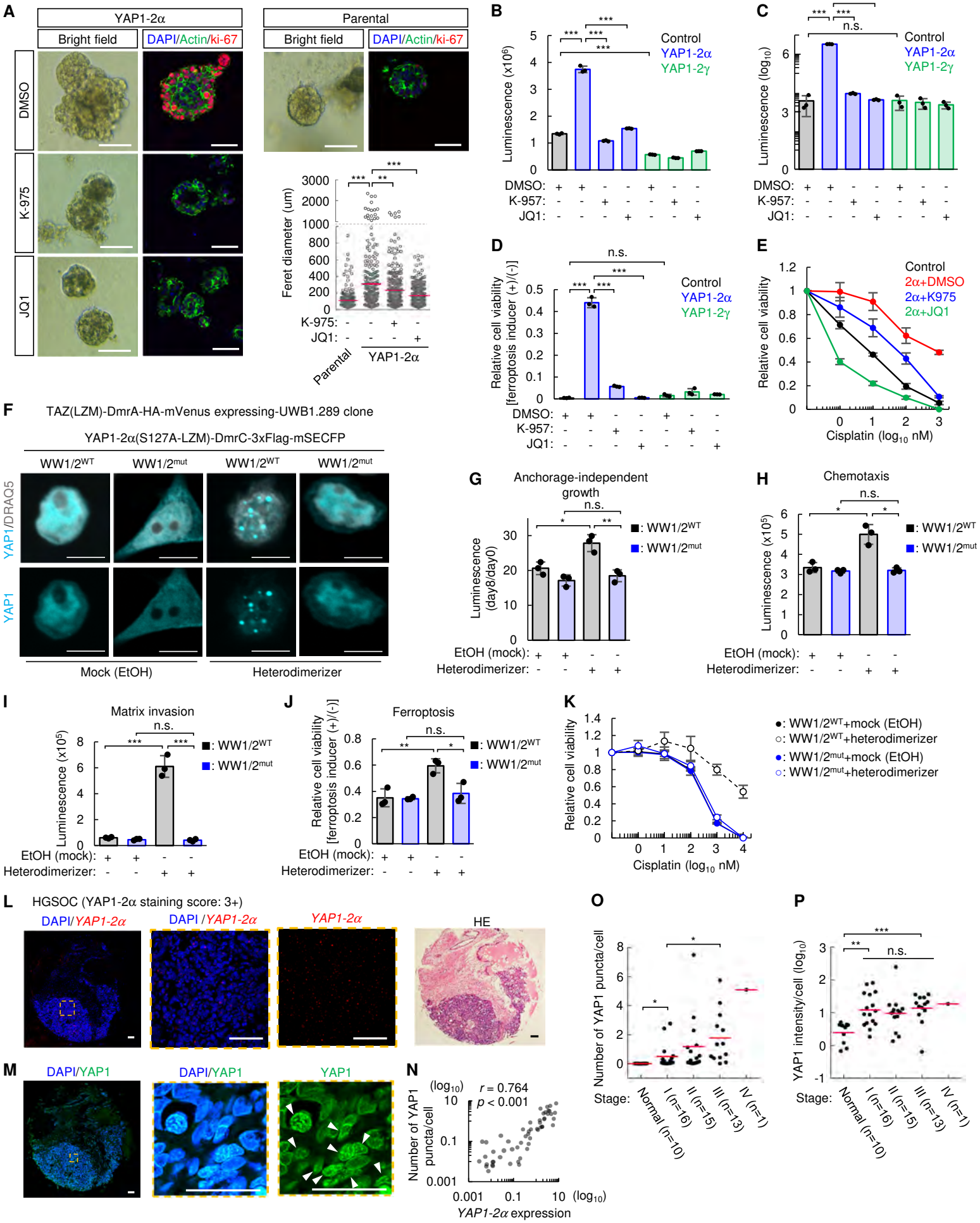
A
YAP1-2α
Parental
Bright field
DAPI/Actin/ki-67
DMSO
K-975
JQ1
Feret diameter (um)
K-975:
JQ1:
Parental
YAP1-2α
B
Luminescence (x10^6)
Control
YAP1-2α
YAP1-2γ
DMSO:
K-957:
JQ1:
C
Luminescence (log10)
n.s.
D
Relative cell viability [ferroptosis inducer (+)/(-)]
E
Relative cell viability
Control
2α+DMSO
2α+K975
2α+JQ1
Cisplatin (log10 nM)
F
TAZ(LZM)-DmrA-HA-mVenus expressing-UWB1.289 clone
YAP1-2α(S127A-LZM)-DmrC-3xFlag-mSECFP
WW1/2WT
WW1/2mut
YAP1/DRAQ5
YAP1
Mock (EtOH)
Heterodimerizer
G
Anchorage-independent growth
Luminescence (day8/day0)
■: WW1/2WT
■: WW1/2mut
EtOH (mock):
Heterodimerizer:
H
Chemotaxis
Luminescence (x10^5)
I
Matrix invasion
J
Ferroptosis
K
Relative cell viability
●: WW1/2WT+mock (EtOH)
○: WW1/2WT+heterodimerizer
●: WW1/2mut+mock (EtOH)
○: WW1/2mut+heterodimerizer
Cisplatin (log10 nM)
L
HGSOC (YAP1-2α staining score: 3+)
DAPI/YAP1-2α
HE
M
DAPI/YAP1
YAP1
N
r = 0.764
p < 0.001
Number of YAP1 puncta/cell
YAP1-2α expression
O
Number of YAP1 puncta/cell
Stage:
Normal (n=10)
I (n=16)
II (n=15)
III (n=13)
IV (n=1)
P
YAP1 intensity/cell (log10)

Figure 7.

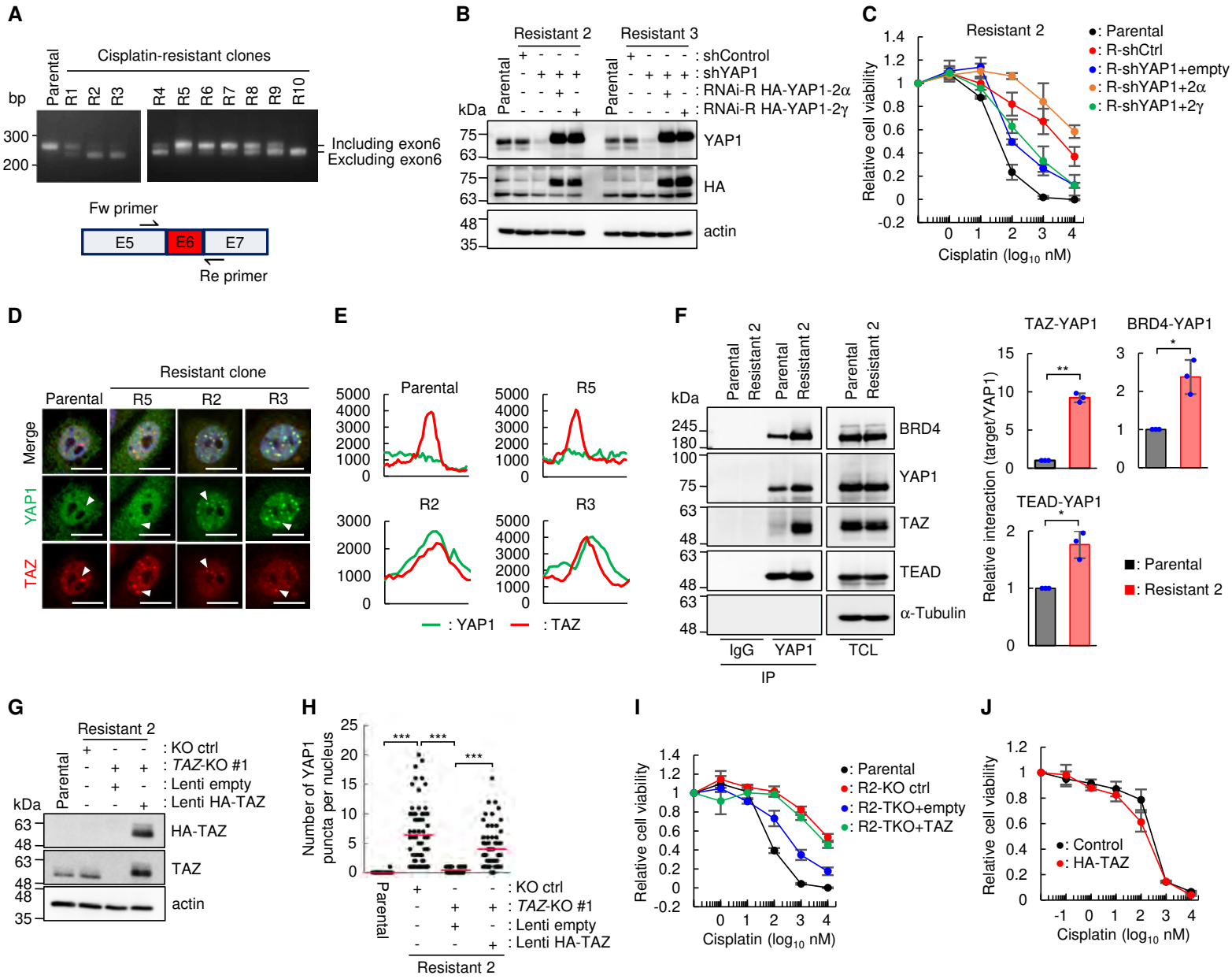
A
Cisplatin-resistant clones
Parental
R1
R2
R3
R4
R5
R6
R7
R8
R9
R10
bp
300
200
Including exon6
Excluding exon6
Fw primer
E5
E6
E7
Re primer
B
Resistant 2
Resistant 3
Parental
: shControl
: shYAP1
: RNAi-R HA-YAP1-2α
: RNAi-R HA-YAP1-2γ
kDa
YAP1
HA
actin
C
Resistant 2
: Parental
: R-shCtrl
: R-shYAP1+empty
: R-shYAP1+2α
: R-shYAP1+2γ
Relative cell viability
Cisplatin (log10 nM)
D
Resistant clone
Parental
R5
R2
R3
Merge
YAP1
TAZ
E
Parental
R5
R2
R3
: YAP1
: TAZ
F
Parental
Resistant 2
kDa
BRD4
YAP1
TAZ
TEAD
α-Tubulin
IgG
YAP1
TCL
IP
TAZ-YAP1
BRD4-YAP1
TEAD-YAP1
Relative interaction (target/YAP1)
: Parental
: Resistant 2
G
Resistant 2
Parental
: KO ctrl
: TAZ-KO #1
: Lenti empty
: Lenti HA-TAZ
kDa
HA-TAZ
TAZ
actin
H
Number of YAP1 puncta per nucleus
Parental
: KO ctrl
: TAZ-KO #1
: Lenti empty
: Lenti HA-TAZ
Resistant 2
I
: Parental
: R2-KO ctrl
: R2-TKO+empty
: R2-TKO+TAZ
Relative cell viability
Cisplatin (log10 nM)
J
: Control
: HA-TAZ
Relative cell viability
Cisplatin (log10 nM)

The YAP1 isoform, YAP1-2α, promotes oncogenic properties by inducing liquid-liquid phase separation through specific heterodimerization with TAZ

Takuya Ooki[1], Takeru Hayashi[1], Yui Yamamoto[1], & Masanori Hatakeyama[1,2,*]

[1]Laboratory of Microbial Carcinogenesis, Institute of Microbial Chemistry, Microbial Chemistry Research Foundation, Tokyo, Japan

[2]Center of Infection-associated Cancer, Institute for Genetic Medicine, Hokkaido University, Sapporo, Japan

*e-mail: mhata@m.u-tokyo.ac.jp

Running title

Molecular Mechanism of LLPS Induction by YAP isoform YAP1-2α

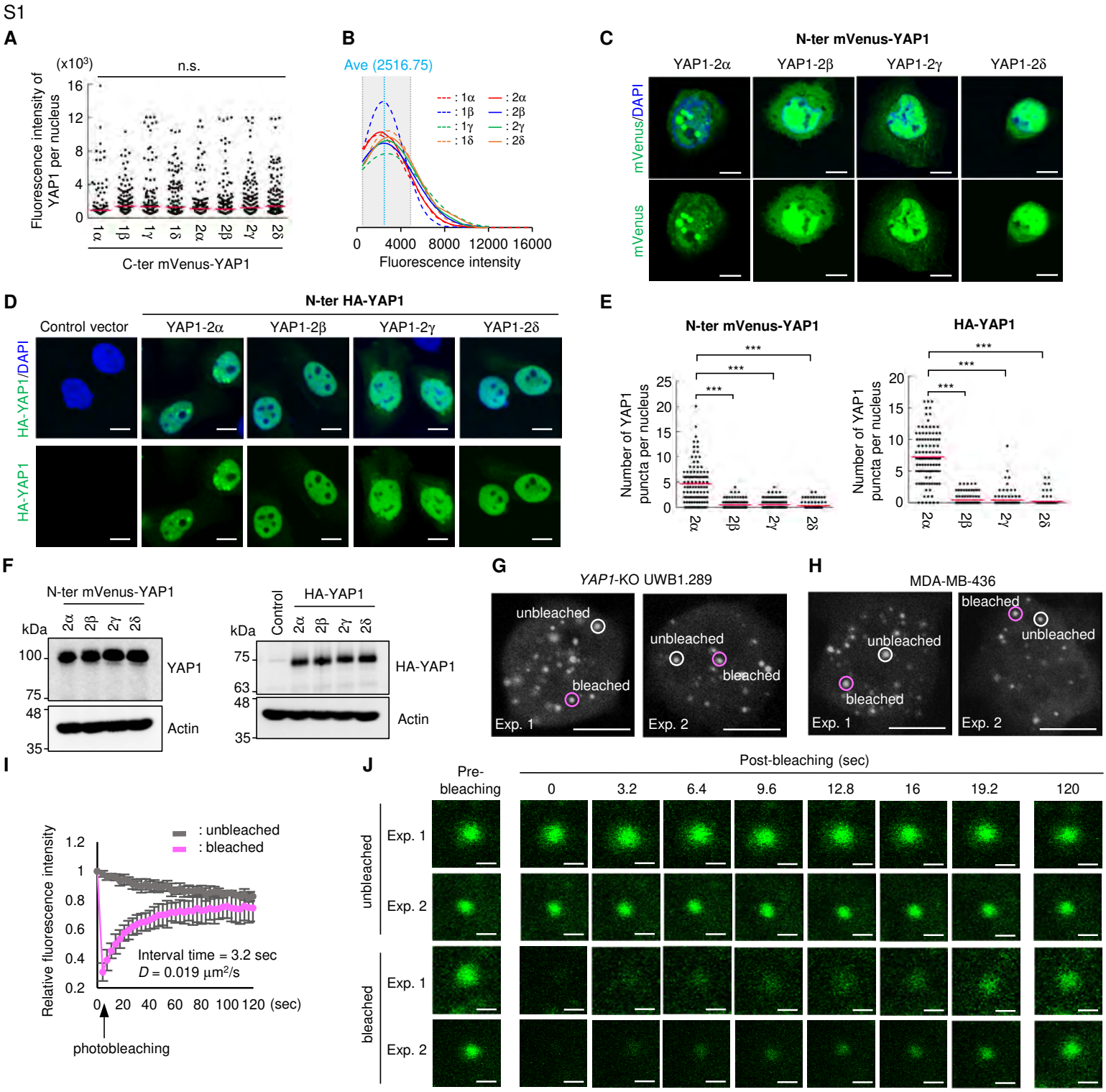

Figure S1. YAP1-2α induces LLPS.

A, The intensity of YAP1 nuclear expression in individual cells was measured using ImageJ (related to Fig. 1*B-D*). Regions of interest (ROIs) were defined based on DAPI staining. mVenus-YAP1-positive cells were selected based on cells with nuclear YAP1 intensity > 500 (n > 100 nuclei in each group). n.s., not significant (ANOVA). Red lines indicate the mean value. *B*, The figure shows the distribution of individual YAP1 expression in Fig. S1*A*. The gray region indicates the range of the mean ± SD of nuclear YAP1 intensity, and the cell population within this region was used for the analysis in Fig. 1*C*. *C-D*, Fluorescence imaging analysis of *YAP1*-KO UWB1.289 cells transfected with a plasmid encoding the indicated YAP1 isoform fused to mVenus © or an HA tag (*D*) at the N-terminus. mVenus fluorescence was detected as a green signal. *E*, The figure shows the number of nuclear YAP1 puncta as indicated in Fig. S1*C* (left panel) or Fig. S1*D* (right panel). n = 100 nuclei in each group. ***p < 0.001 (Mann-Whitney U test). Red lines indicate the mean value. *F*, Immunoblotting analysis using the indicated antibodies (related to Fig. S1*C*; left, and Fig. S1*D*; right). *G*, Entire nuclear images of cells used for FRAP analysis (related to Fig. 1*I*). Two different cells were labeled as Exp. 1 and Exp. 2. White circles indicate non-photobleached puncta. Pink circles indicate photobleached puncta. *H-J*, FRAP analysis of MDA-MB-436 cells expressing mVenus-fused YAP1-2α. Entire nuclear images of cells used for FRAP analysis (*H*). Fluorescence intensities of puncta (photobleached; n = 5, unbleached; n = 5) obtained from a series of time-lapse images were analyzed. *D* indicates the diffusion coefficient. Error bars indicate mean ± SD (*I*). Representative time-lapse images. Scale bars indicate 1 μm (*J*). (*C-D*, *G-H*) Scale bars indicate 10 μm.

S2-1

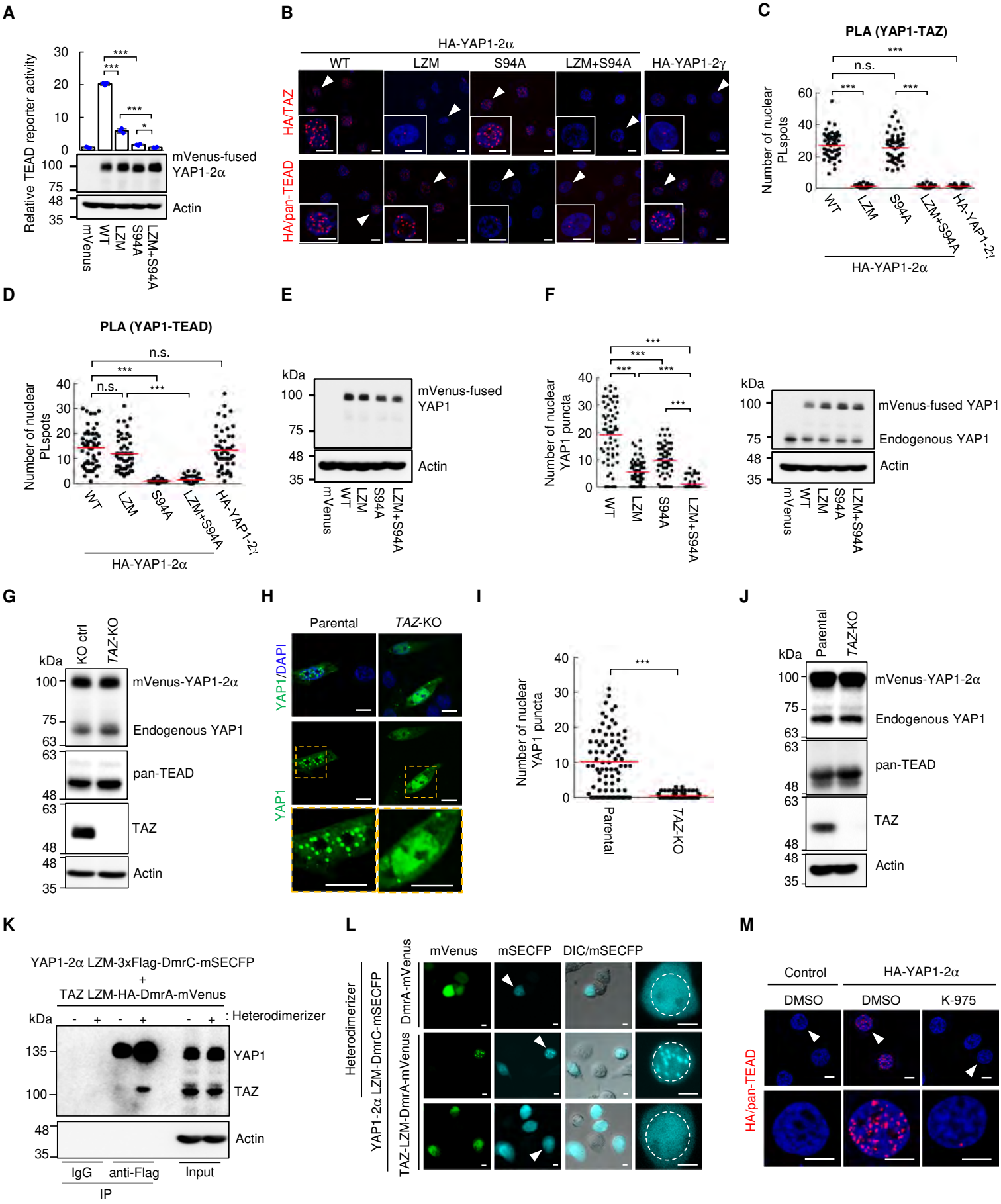
A
Relative TEAD reporter activity
mVenus-fused YAP1-2α
Actin
mVenus
WT
LZM
S94A
LZM+S94A
B
HA-YAP1-2α
WT
LZM
S94A
LZM+S94A
HA-YAP1-2γ
HA/TAZ
HA/pan-TEAD
C
PLA (YAP1-TAZ)
Number of nuclear PLspots
n.s.
HA-YAP1-2α
D
PLA (YAP1-TEAD)
Number of nuclear PLspots
n.s.
HA-YAP1-2α
E
kDa
mVenus-fused YAP1
Actin
F
Number of nuclear YAP1 puncta
kDa
mVenus-fused YAP1
Endogenous YAP1
Actin
G
KO ctrl
TAZ-KO
kDa
mVenus-YAP1-2α
Endogenous YAP1
pan-TEAD
TAZ
Actin
H
Parental
TAZ-KO
YAP1/DAPI
YAP1
I
Number of nuclear YAP1 puncta
Parental
TAZ-KO
J
Parental
TAZ-KO
kDa
mVenus-YAP1-2α
Endogenous YAP1
pan-TEAD
TAZ
Actin
K
YAP1-2α LZM-3xFlag-DmrC-mSECFP
+
TAZ LZM-HA-DmrA-mVenus
kDa
: Heterodimerizer
YAP1
TAZ
Actin
IgG
anti-Flag
Input
IP
L
mVenus
mSECFP
DIC/mSECFP
Heterodimerizer
YAP1-2α LZM-DmrC-mSECFP
DmrA-mVenus
TAZ-LZM-DmrA-mVenus
M
Control
HA-YAP1-2α
DMSO
DMSO
K-975
HA/pan-TEAD

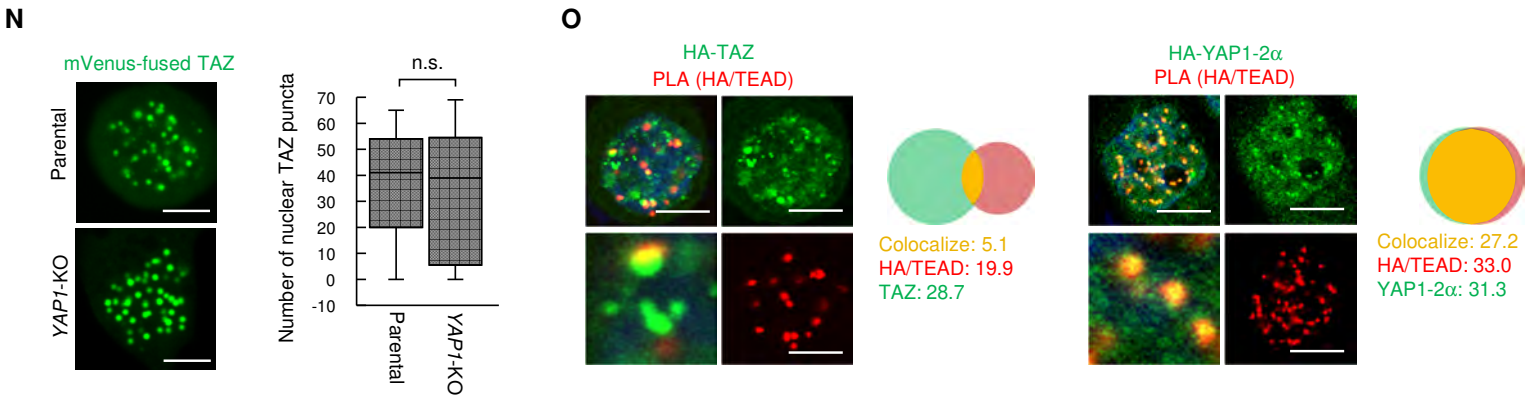

Figure S2. The YAP1-2α/TAZ/TEAD enhancer complex is required for LLPS formation

A, TEAD reporter assay of YAP1-2α mutants in *YAP1*-KO UWB1.289 cells (top). Error bars indicate the mean ± SD, n = 3 (technical replicates). Each plot shows relative luciferase activity per well. Expression of the YAP1-2α mutant proteins (bottom). *B*, Interaction of YAP1-2α with endogenous TAZ (top) or TEAD (bottom) in UWB1.289 cells was visualized as PL spots (red) using PLA. Nuclei indicated by white arrows are magnified. *C-D*, The number of nuclear PL spots is shown in the graph (*C*: interaction between HA-YAP1-2α and TAZ, *D*: interaction between HA-YAP1-2α and TEAD). n = 50 nuclei in each group. *E*, Related to Fig.2*B*. Expression of the indicated proteins in *YAP1*-KO UWB1.289 cells was confirmed by immunoblotting. *F*, Nuclear puncta formation in MDA-MB-436 cells expressing mVenus-YAP1-2α mutants. Number of YAP1 puncta in the nucleus (left). n = 60 nuclei in each group. Protein expression shown by immunoblotting (right). *G*, Related to Fig. 2*C*. Immunoblotting analysis of *TAZ*-KO UWB1.289 cells expressing mVenus-YAP1-2α using the indicated antibodies. *H-J*, *TAZ*-KO MDA-MB-436 cells were transfected with an mVenus-fused YAP1-2α vector. Fluorescence images (*H*). Number of YAP1-2α puncta in the nucleus. n = 80 cells per group were obtained from three biological replicate experiments (*I*). Confirmation of TAZ knockout, mVenus-YAP1-2α expression, and TEAD expression by immunoblotting (*J*). *K-L*, Related to Fig. 2*D-E,* Confirmation of heterodimer formation between the indicated proteins upon treatment with heterodimerizer (*K*) and immunofluorescence images (*L*). DIC: differential interference contrast image. *M*, Inhibition of the physical interaction between HA-YAP1-2α and endogenous TEAD by K-975 in UWB1.289 cells was detected using PLA. *N*, Effect of *YAP1* knockout on TAZ/TAZ LLPS in UWB1.289 cells. TAZ/TAZ LLPS (left). Number of nuclear TAZ puncta in Parental or *YAP1*-KO cells (right). Boxes include the 25th–75th percentiles with bars indicating medians. n = 13 cells for each group. *O*, Interaction of YAP1-2α or TAZ with TEAD in UWB1.289 cells was visualized using PLA following immunofluorescence staining. Co-localization of PL spots and YAP1-2α or TAZ puncta. Green circle: number of YAP1-2α or TAZ puncta, Red circle: number of nuclear PL spots, Yellow circle: number of colocalized spots. n = 15 nuclei. All scale bars represent 10 µm. (*A*, *C*, *D, F*, *I*, *N*) ***p < 0.001; *p < 0.05; n.s., not significant (*A*: Student's t test; *C*, *D*, *F*, *I*, *N*: Mann-Whitney U test). (*C*, *D*, *F*, *I*) Red lines indicate the mean.

S3-1

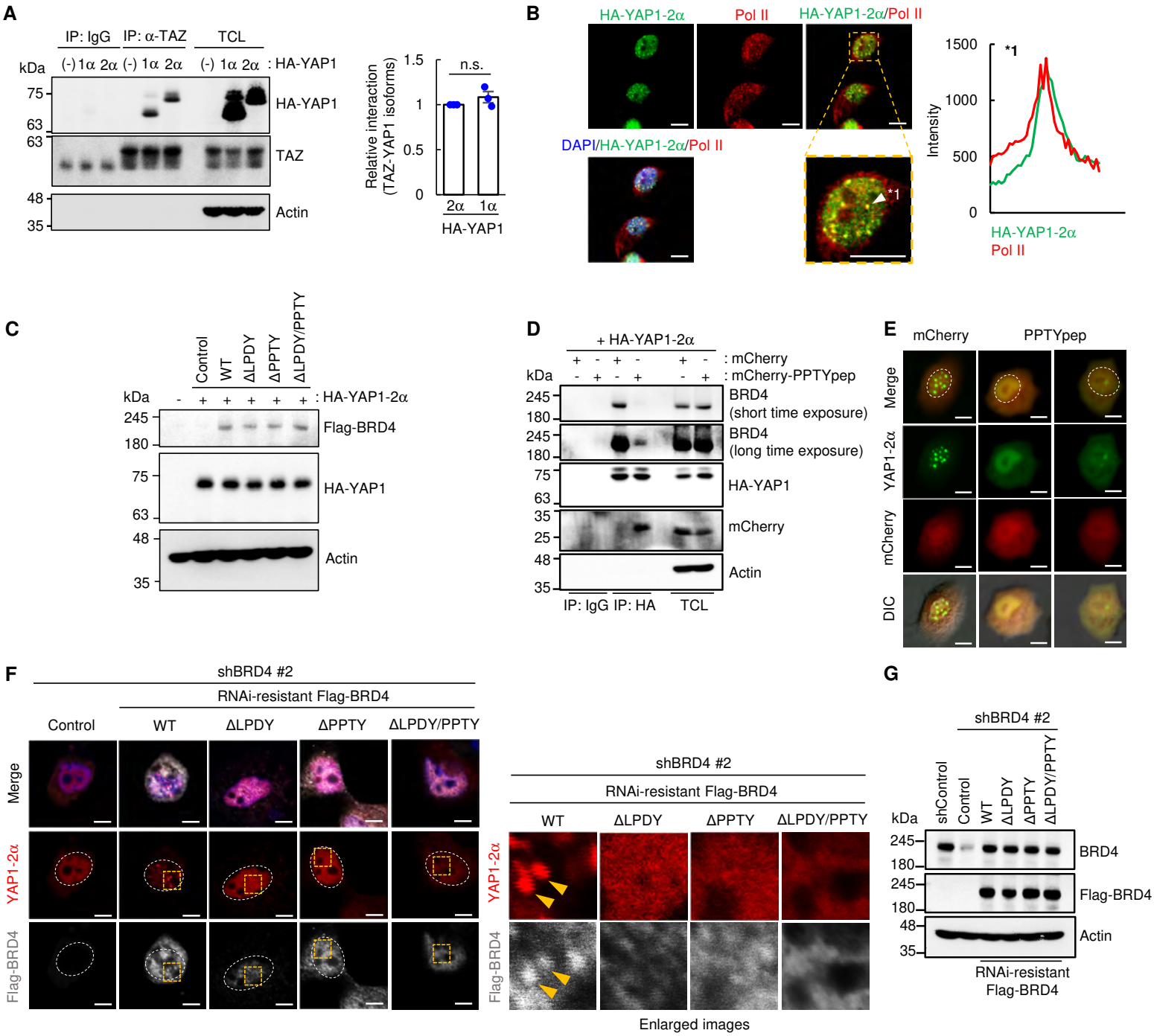
A
IP: IgG
IP: α-TAZ
TCL
kDa
(-) 1α 2α (-) 1α 2α (-) 1α 2α : HA-YAP1
75
63
63
48
35
HA-YAP1
TAZ
Actin
Relative interaction (TAZ-YAP1 isoforms)
1.5
1
0.5
0
n.s.
2α
1α
HA-YAP1
B
HA-YAP1-2α
Pol II
HA-YAP1-2α/Pol II
DAPI/HA-YAP1-2α/Pol II
*1
Intensity
1500
1000
500
0
HA-YAP1-2α
Pol II
C
Control
WT
ΔLPDY
ΔPPTY
ΔLPDY/PPTY
kDa
: HA-YAP1-2α
245
180
75
63
48
35
Flag-BRD4
HA-YAP1
Actin
D
+ HA-YAP1-2α
: mCherry
: mCherry-PPTYpep
kDa
245
180
245
180
75
63
35
25
48
35
BRD4 (short time exposure)
BRD4 (long time exposure)
HA-YAP1
mCherry
Actin
IP: IgG
IP: HA
TCL
E
mCherry
PPTYpep
Merge
YAP1-2α
mCherry
DIC
F
shBRD4 #2
RNAi-resistant Flag-BRD4
Control
WT
ΔLPDY
ΔPPTY
ΔLPDY/PPTY
Merge
YAP1-2α
Flag-BRD4
Enlarged images
G
shBRD4 #2
shControl
Control
WT
ΔLPDY
ΔPPTY
ΔLPDY/PPTY
kDa
245
180
245
180
48
35
BRD4
Flag-BRD4
Actin
RNAi-resistant Flag-BRD4
H
HA-YAP1-2α
WT
WW1mut
WW2mut
WW1/2mut
HA/DAPI
HA
I
HA-YAP1-2α
Control
WT
WW1mut
WW2mut
WW1/2mut
kDa
75
63
48
35
HA-YAP1
actin
J
HA-YAP1-2α (S127A)
Control
WT
WW1mut
WW2mut
WW1/2mut
kDa
75
63
48
35
HA-YAP1
actin

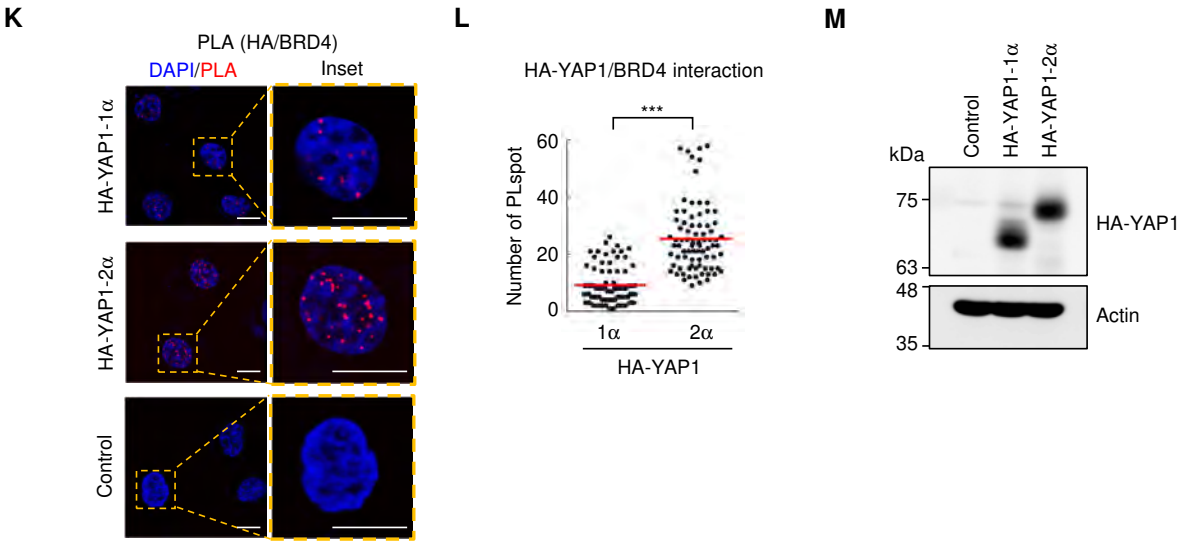

Figure S3. WW domain-mediated multiple interactions between YAP1-2α and BRD4 are important for YAP1 LLPS formation
A, Interactions between TAZ and YAP1-1α or YAP1-2α in MDA-MB-436 cells were examined by an anti-HA immunoblotting analysis of the anti-TAZ immunoprecipitates (left). The relative interaction between YAP1-1α and TAZ was calculated by setting YAP1-2α intensity per TAZ intensity in the IP sample to one (right). n = 3 (biological replicates), n.s., not significant (Student's t test). Error bars indicate SEM. *B*, Immunofluorescence images of HA-YAP1-2α (green) and Pol II (red) (left panel). Colocalization of YAP1-2α and Pol II in the puncta is shown with a white arrow. The graph shows the fluorescence intensities of HA-YAP1-2α and Pol II in the YAP1 puncta indicated by a white arrow (right panel). *C*, Related to Fig. 3*C*. Expression levels of HA-YAP1-2α and Flag-BRD4 mutants were determined by immunoblotting. *D*, Competitive inhibition of the YAP1-2α/BRD4 interaction using an mCherry-fused PPTY peptide derived from the BRD4 sequence (PPTYpep). HA-YAP1-2α-expressing cells were transfected with the mCherry or PPTYpep vector and subjected to a sequential immunoprecipitation-immunoblotting experiment using the indicated antibodies. *E*, Inhibition of YAP1-2α puncta formation using PPTYpep, which interferes with the YAP1-2α/BRD4 interaction. *F-G*, Related to Fig. 3*F*. Genetic rescue of the shBRD4-mediated reduction in YAP1-2α puncta formation by shBRD4-resistant BRD4. Immunofluorescence images of YAP1-2α (red), Flag-BRD4 (gray) and nuclei (blue). The area indicated by the yellow dashed box is enlarged (right panels). Yellow arrows indicate the colocalization of YAP1-2α puncta and BRD4 (*F*). Confirmation of shBRD4 (#2)-resistant Flag-BRD4 mutants and BRD4 knockdown efficiency by immunoblotting (*G*). *H-I*, UWB1.289 cells were infected with lentivirus transducing HA-YAP1-2α(WT), HA-YAP1-2α(WW1^{mut}), HA-YAP1-2α(WW2^{mut}), or HA-YAP1-2α(WW1/2^{mut}). Immunofluorescence staining of HA-YAP1-2α WW domain mutants (green) (*H*). Expression levels of HA-YAP1-2α WW domain mutants were determined by immunoblotting (*I*). *J*, Related to Fig. 3*G-H*. Expression levels of HA-YAP1-2α(S127A) WW domain mutants were confirmed by immunoblotting. *K-M*, *YAP1*-KO UWB1.289 cells infected with the lentivirus transducing the indicated HA tagged-YAP1 isoform. Analysis of the binding capacity of the YAP1-1α and YAP1-2α to BRD4 using PLA (*K*). Red dots: PL spots (HA-YAP1/BRD4 interaction), blue: nucleus. Statistical analysis of Figure. S3*K* is shown in the graph (*L*). ***$p < 0.001$ (Mann-Whitney U test), n = 80 nuclei for each group. Red bars indicate the mean value. Expression levels of HA-YAP1-1α and HA-YAP1-2α were determined by immunoblotting (*M*). All scale bars represent 10 μm.

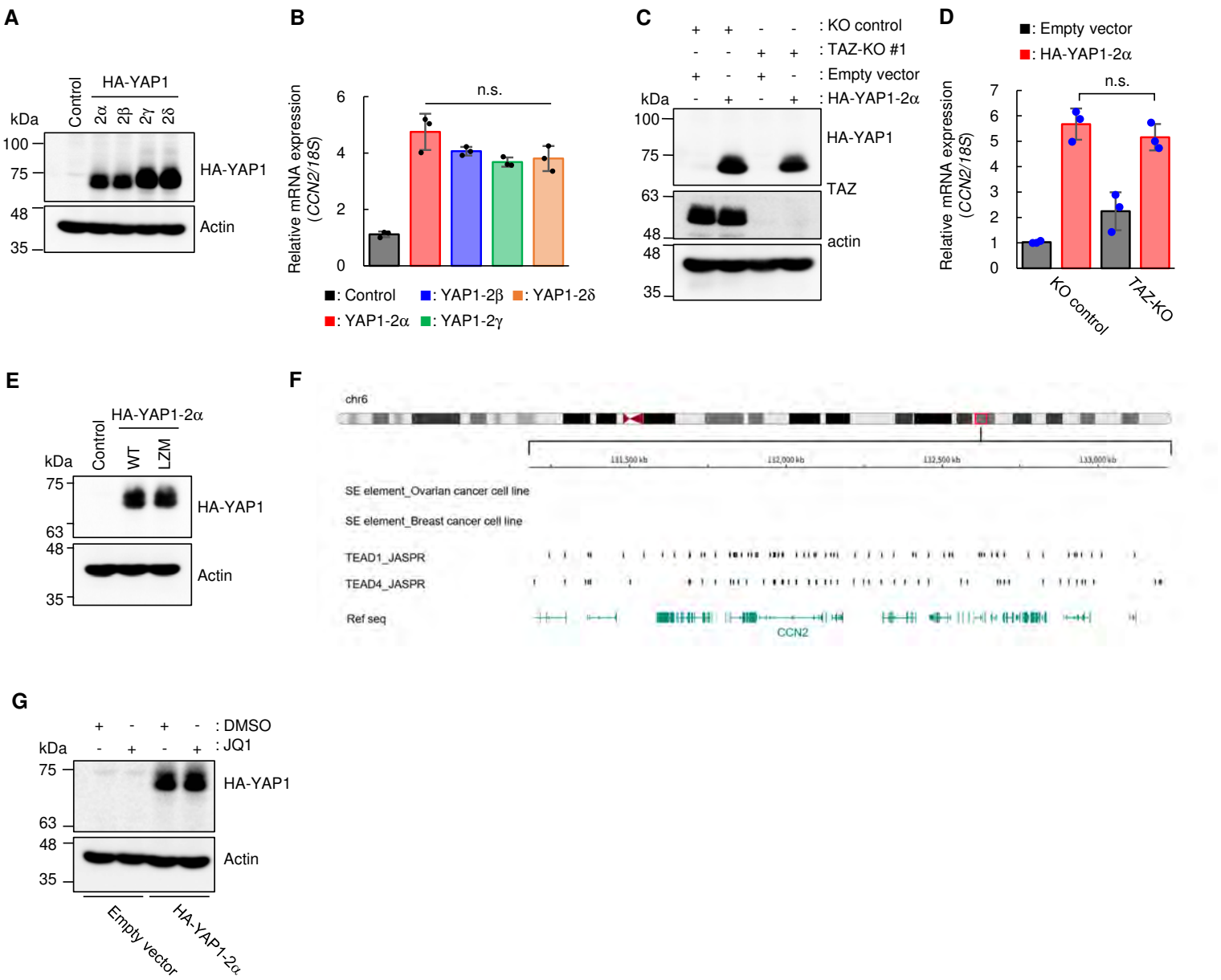

Figure S4. YAP1-2α regulates gene expression in a heterodimerization-dependent manner with TAZ

A-B, Related to Fig. 4*A*. Protein expression levels of the HA-YAP1 isoforms were detected by immunoblotting (*A*). The expression level of the typical TEAD target gene (*CCN2*) was analyzed by qPCR (*B*). *C-D*, Related to Fig. 4*B*. Protein expression levels of the HA-YAP1-2α and TAZ knockout were confirmed by immunoblotting (*C*). The expression level of the typical TEAD target gene (*CCN2*) was analyzed by qPCR (*D*). *E*, Related to Fig. 4*C*. Protein expression levels of the HA-YAP1-2α(WT) and (LZM) were confirmed by immunoblotting. *F*, Prediction of potential TEAD-binding super-enhancer elements around the *CCN2* gene. The identified super-enhancer elements in serous ovarian cancer cells (GSM3328052: PEO1 cells) and triple-negative breast cancer cells (GSM6132824: MDA-MB-436 cells) are shown in the first and second lines from the top. The TEAD-binding motif sequences were predicted using JASPR. There are no potential TEAD-positive super-enhancer elements in the vicinity of the *CCN2* gene. *G*, Related to Fig. 4*I*. Protein expression levels of the HA-YAP1-2α were confirmed by immunoblotting. (*B*, *D*) n.s., not significant (Welch's t test). Error bars indicate the mean ± SD, n = 3 (technical replicates). Plots indicate RQ (relative quantification) for each sample.

S5

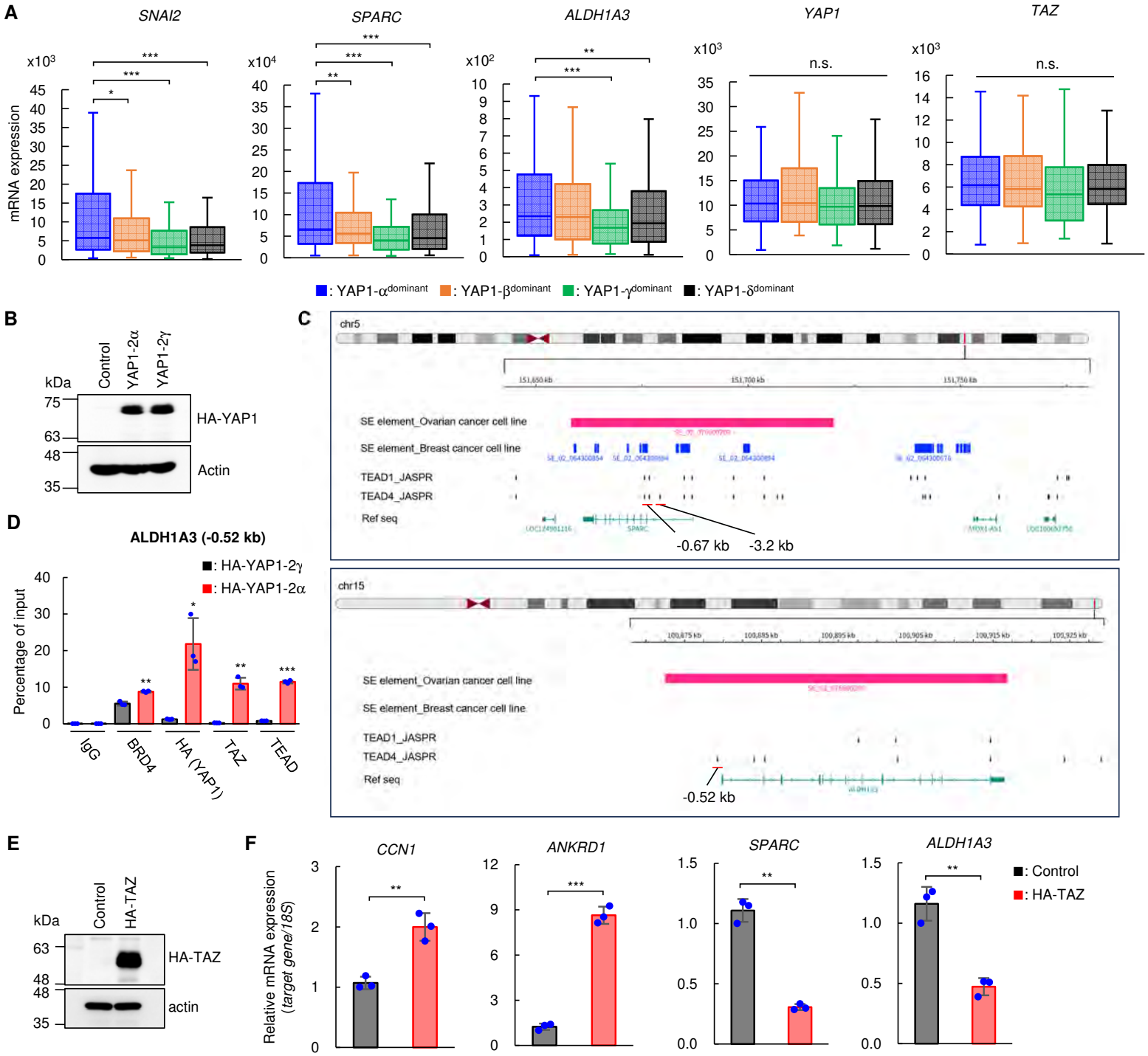

Figure S5. YAP1-2α/TAZ/TEAD super-enhancer activates EMT related genes.
A, Related to Fig. 5*A*-*B*. The mRNA expression levels of EMT related genes (*ZEB1*, *SNAI2*, *SPARC*, *ALDH1A3*), *YAP1*, and *TAZ* in HGSOC patients subdivided by YAP1 isoforms are shown in box-and-whisker plots. The boxes include the 25th–75th percentiles, with bars indicating the means and whiskers indicating data range. ***p < 0.001; **p < 0.01; *p < 0.05; n.s., not significant (Welch's t test). *B*, UWB1.289 cells transduced with the indicated YAP1 isoforms using lentiviruses. Protein expression levels of the HA-YAP1 isoforms were detected by immunoblotting. *C*, The identified super-enhancer elements in serous ovarian cancer cells (GSM3328052) and triple-negative breast cancer cells (GSM6132824) are shown in the first and second lines from the top. The TEAD-binding motif sequences were predicted using JASPR. Upstream of *SPARC* (top panel), and upstream of *ALDH1A3* (bottom panel). The region where primers for ChIP-qPCR were designed is indicated by a red line. *D*, Related to Fig. 5*E*. The enrichment levels of the super-enhancer marker BRD4, YAP1 (HA-tag), TAZ, and TEAD at the potential super-enhancer element upstream of *ALDH1A3*, indicated by the red line in panel *C* (bottom panel), were evaluated using qPCR. The DNA templates were prepared using CUT & RUN with the indicated antibodies. *E*-*F*, Overexpression of TAZ in UWB1.289 cells. Immunoblotting analysis using the indicated antibodies (*E*). Verification of the effects of TAZ overexpression through qPCR analysis of typical TEAD target genes (*CCN1*, *ANKRD1*), *SPARC*, and *ALDH1A3* (*F*). (*D*, *F*) ***p < 0.001; **p < 0.01, *p < 0.05 (Welch's t test). Error bars indicate the mean ± SD. n = 3 (technical replicates).

S6-1

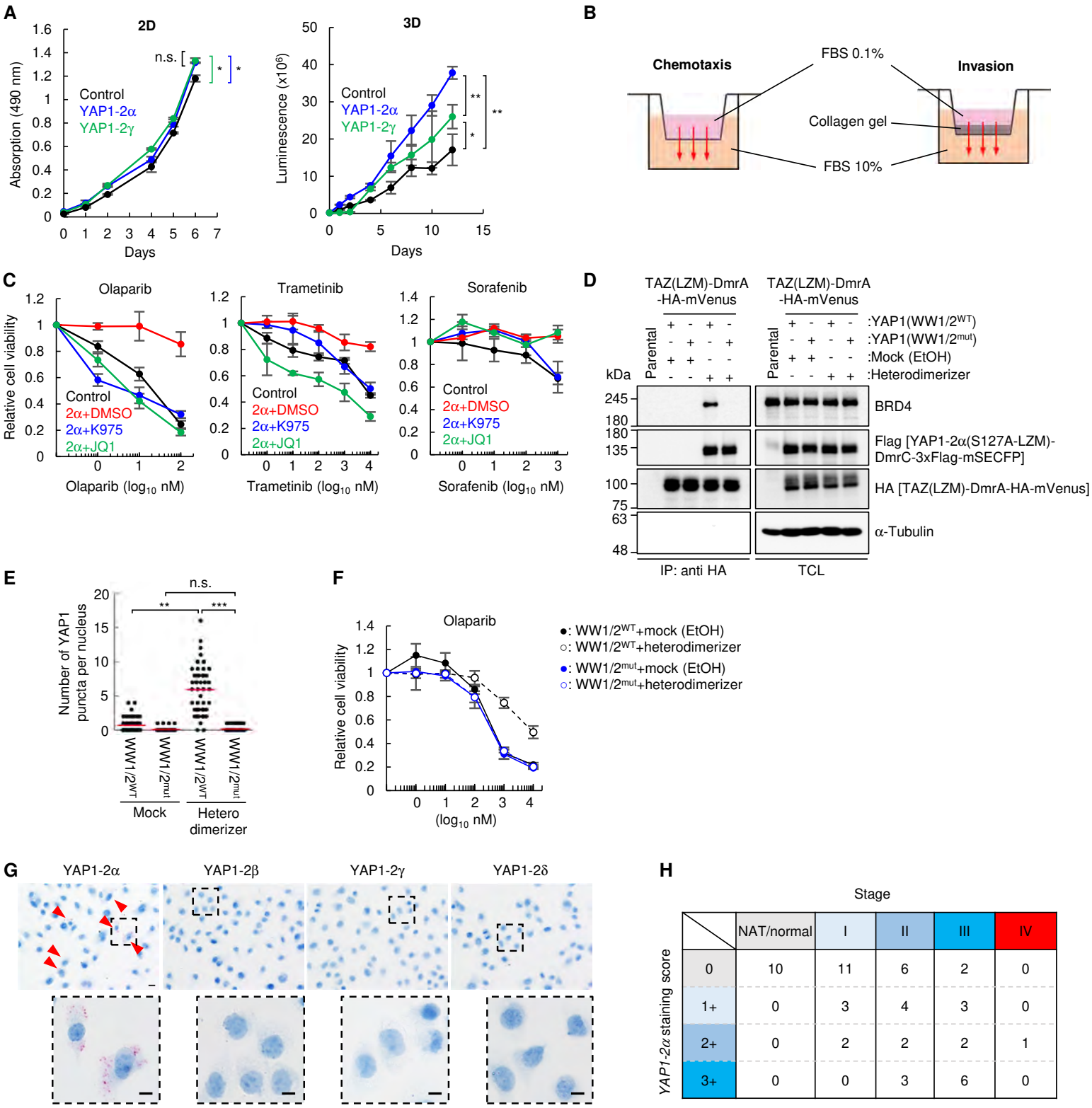

YAP1-2α staining score	NAT/normal	I	II	III	IV
0	10	11	6	2	0
1+	0	3	4	3	0
2+	0	2	2	2	1
3+	0	0	3	6	0

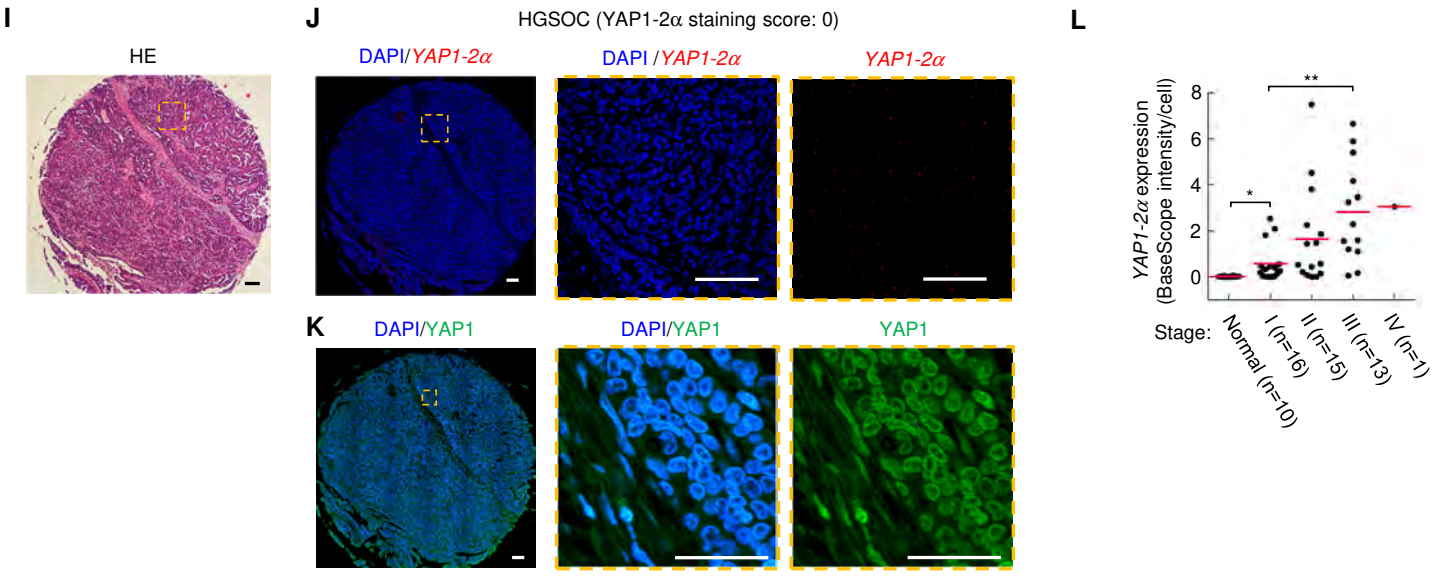

Figure S6. YAP1-2α contributes to the acquisition of malignant properties in cancer.
A, Two-dimensional or three-dimensional cell proliferation of YAP1-2α-overexpressing, YAP1-2γ-overexpressing, or control UWB1.289 cells. Two-dimensional cell proliferation was measured by an MTS assay (*left*). Anchorage-independent 3D cell growth was evaluated by measuring ATP content (*right*). B, Related to Fig. 6*B-C*. Schematic view of chemotaxis assay (*left*) and matrix invasion assay (*right*). *C*, The effect of the YAP1-2α/TAZ/TEAD super-enhancer on the sensitivity of UWB1.289 cells to various anticancer drugs. Cells were treated with JQ1 or K-975 along with the listed reagent. As a mock control, cells were treated with DMSO. Olaparib (PARP inhibitor), Trametinib (MEK inhibitor), and Sorafenib (tyrosine kinase inhibitor). *D-F*, Related to Fig. 6*F-K*. UWB1.289 clone cells expressing TAZ(LZM)-DmrA-HA-mVenus were infected with lentivirus transducing YAP1-2α(S127A-LZM)-DmrC-3xFlag-mSECFP-WW1/2^{WT} or YAP1-2α(S127A-LZM)-DmrC-3xFlag-mSECFP-WW1/2^{mut} and further treated with heterodimerizer or mock control (ethanol). Heterodimerization between YAP1 and TAZ, as well as co-immunoprecipitation of BRD4 were examined by immunoblotting analysis of anti-HA immunoprecipitates. Total cell lysates (TCL) were used as input samples (*D*). Statistical analysis of Figure. 6*F*. n = 45 nuclei per group; ***p < 0.001; **p < 0.01; n.s., not significant (Mann-Whitney U test). Red lines indicate the mean value (*E*). Sensitivity to Olaparib was measured by an MTS assay (*F*). *G*, Confirmation of BaseScope probe specificity for the *YAP1-2α* isoform. BaseScope was performed in cells transfected with the indicated YAP1 isoforms. Red arrows indicate BaseScope signal-positive cells. Scale bars represent 10 µm. *H*, Table of tumor progression stage and *YAP1-2α* staining score. *I-L*, Related to Figure 6*L-P*. Analysis of HGSOC tissue arrays. HE staining (*I*), BaseScope signals (*YAP1-2α* mRNA) (*J*), and YAP1 immunofluorescence staining (*K*) in an HGSOC patient with low *YAP1-2α* expression (*YAP1-2α* staining score: 0). Nuclei were stained with DAPI. The dashed box area was enlarged. Scale bars represent 100 µm. The correlation between clinical stage and *YAP1-2α* mRNA expression levels (BaseScope intensity per cell) is shown in graph (*L*). **p < 0.01; *p < 0.05 (Welch's t test). Red lines indicate the mean value.

S7

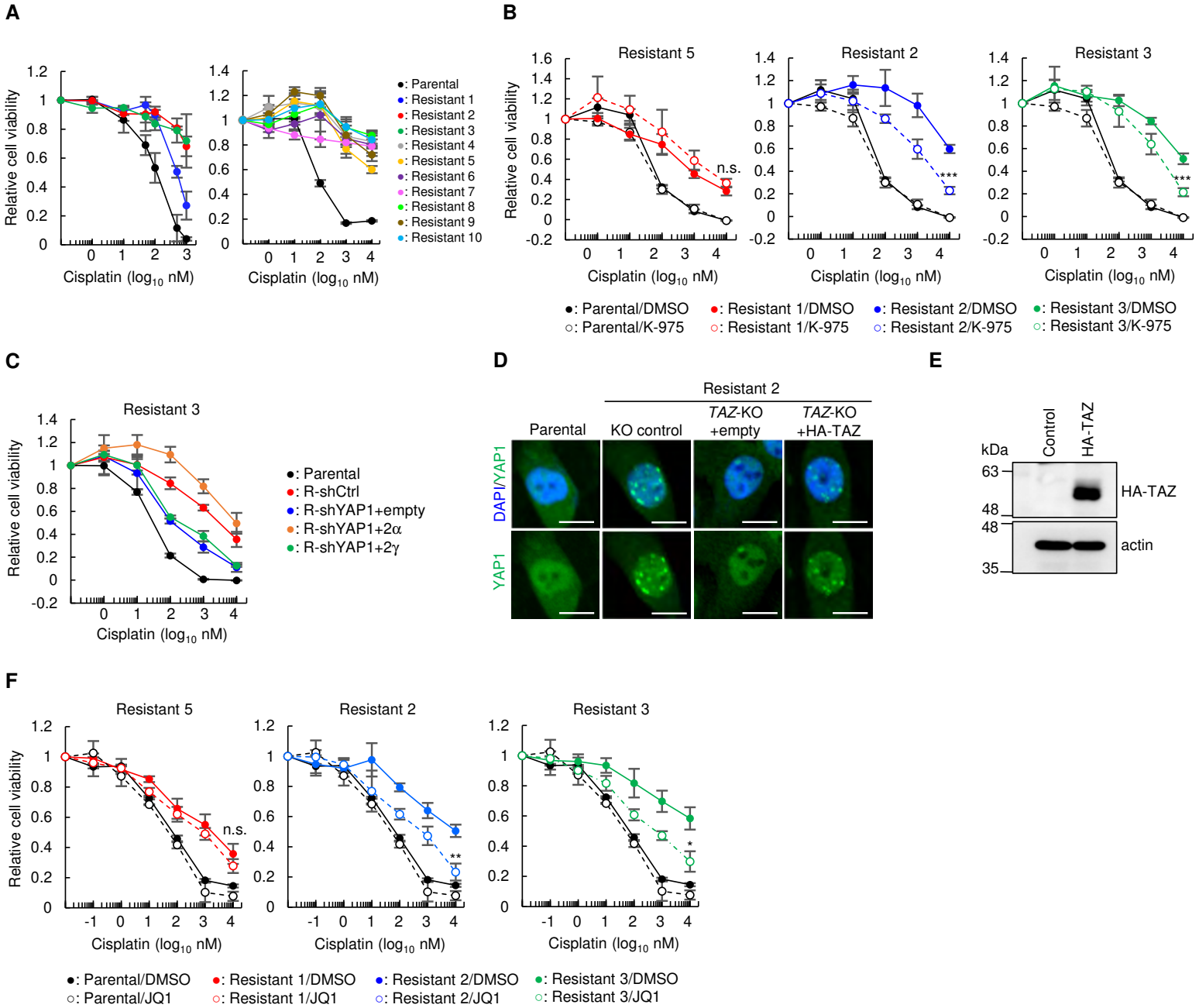

Figure S7. Inhibiting the formation of the YAP1-2α/TAZ/TEAD/BRD4 complex restores sensitivity to Cisplatin .
A, Sensitivity to Cisplatin in established independent Cisplatin-resistant clones was assessed by an MTS assay. *B*, The effect of K-975 treatment on the Cisplatin sensitivity of the indicated Cisplatin-resistant clone cells was measured using an MTS assay. *C*, Related to Fig. 7*B*-*C*. The sensitivity of the indicated cells to Cisplatin was evaluated by an MTS assay. *D*, Related to Fig. 7*H*. Effect of *TAZ*-knockout on endogenous YAP1 puncta formation in Cisplatin-resistant clone 2 (resistant 2). Immunofluorescence imaging of YAP1 (green). *E*, Related to Fig. 7*J*. HA-TAZ expression was confirmed by immunoblotting. *F*, The effect of JQ1 treatment on the Cisplatin sensitivity of the indicated Cisplatin-resistant clone cells was measured by an MTS assay. (*B*, *F*) DMSO was used as a mock control. ***p < 0.001; **p < 0.01; *p < 0.05; n.s., not significant (Student's t test), n=3 (three technical replicates).

Table S1. Primer sequences for qRT-PCR

Gene name	Primer sequence
Human *CCN1* Forward	5'-CTCACTGAAGCGGCTCCCTGTTTT-3'
Human *CCN1* Reverse	5'-GGGTTTCTTTCACAAGGCGGCACT-3'
Human *CCN2* Forward	5'-GTGTGACGAGCCCAAGGACCAAAC-3'
Human *CCN2* Reverse	5'-GAGGCGTTGTCATTGGTAACCCGG-3'
Human *ANKRD1* Forward	5'-TGCTTGAATCCACAGCCATCCACT-3'
Human *ANKRD1* Reverse	5'-TCTGTCTTTGGCGTTGAGGTCTGC-3'
Human *SPARC* Forward	5'-GTGTGCAGCAATGACAACAAGACC-3'
Human *SPARC* Reverse	5'-GAATTCGGTCAGCTCAGAGTCCAG-3'
Human *ALDH1A3* Forward	5'-ATGGAAGACAAGGGGCTCTTCATC-3'
Human *ALDH1A3* Reverse	5'-AGAAGCCAACTTCAGGGCTTTGTC-3'
Human *SNAI2* Forward	5'-CGGACCCACACATTACCTTGTGTT-3'
Human *SNAI2* Reverse	5'-ATCAGAATGGGTCTGCAGATGAGC-3'
ChIP-qPCR for human *CCN1* (-0.3 kb) Forward	5'-CAAAGGTGCAATGGAGCCAGG-3'
ChIP-qPCR for human *CCN1* (-0.3 kb) Reverse	5'-GAGGCGCCGCGTGTTGCAG-3'
ChIP-qPCR for human *CCN1* (-0.85 kb) Forward	5'-CTTTGGGACTTGTTCCGAACACG-3'
ChIP-qPCR for human *CCN1* (-0.85 kb) Reverse	5'-TGACCGGGCAGCCACTGAAGC-3'
ChIP-qPCR for human *ALDH1A3* (-0.52 kb) Forward	5'-AGCAGGGCACGTGCGCAGC-3'
ChIP-qPCR for human *ALDH1A3* (-0.52 kb) Reverse	5'-CACATGCAGCCCACTCCCAG-3'
ChIP-qPCR for human *SPARC* (-0.67 kb) Forward	5'-CTTCCTCCTCTGTCGCCTCCTC-3'
ChIP-qPCR for human *SPARC* (-0.67 kb) Reverse	5'-GAGAAAAATGTGGCCACCCTCA-3'
ChIP-qPCR for human *SPARC* (-3.2 kb) Forward	5'-AAACTGCCAACGGCTAACAGCA-3'
ChIP-qPCR for human *SPARC* (-3.2 kb) Reverse	5'-CCAGGAACTCAGGCCAGTTCAA-3'

Table S2. shRNA or sgRNA sequences

	Target gene	Sequence (Sence)
shControl	non-target (SIGMA, Cat #SHC216)	GCGCGAUAGCGCUAAUAAUUU
shBRD4 #1	NM_058243	GCUCAAGACACUAUGGAAACA
shBRD4 #2	NM_058243	GGUACCAAACACAACUCAAGC
shTAZ	NM_015472	ACGUUGACUUAGGAACUUU
shYAP1	NM_001130145	GACAUCUUCUGGUCAGAGAU
sgTAZ	NM_015472	ATCCGAAGCCTAGCTCGTGG
sgYAP1	NM_001130145	GCATCAGATCGTGCACGTCCG